

1   **Coping with extremes: How Epigenetic and Molecular Adaptations Enable**  
2   **Earthworms to Thrive in Volcanic Soils**

3   Rimington, O.<sup>1†</sup>, Novo, M.<sup>2†</sup>, Hodson, M.E.<sup>3</sup>, Camarinho, R<sup>4</sup>., Viveiros, F<sup>4,7</sup>., Silva C<sup>4</sup>, Arruda,  
4   H<sup>4</sup>., Rodrigues A.S.<sup>4,7</sup>, Bruford, M.<sup>1</sup>, Short, S.<sup>1,5</sup>, Morgan, A.J. <sup>1</sup>, Spurgeon, D.<sup>5</sup>, Kille, P. <sup>1</sup> and  
5   Cunha, L.<sup>6\*</sup>

6   <sup>1</sup> School of Biological Science, Cardiff University, Cardiff, United Kingdom

7   <sup>2</sup> Biodiversity, Ecology and Evolution Department. Biological Sciences Faculty. Complutense  
8   University of Madrid, Spain.

9   <sup>3</sup> Department of Environment and Geography, University of York, York, United Kingdom

10   <sup>4</sup> Research Institute of Volcanology and Risks Assessment (IVAR), University of the Azores,  
11   Ponta Delgada, Portugal

12   <sup>5</sup> UK Centre for Ecology and Hydrology, Wallingford, United Kingdom

13   <sup>6</sup>Centre for Functional Ecology, Associate Laboratory TERRA, Department of Life Sciences,  
14   University of Coimbra, 3000-456 Coimbra, Portugal

15   <sup>7</sup> Faculty of Sciences and Technology, University of the Azores, 9501-801 Ponta Delgada,  
16   Portugal

17   <sup>8</sup> Centro de Informação e Vigilância Sismovulcânica dos Açores, Ponta Delgada, Portugal;

18   † These authors contributed equally to this work.

19   \*Correspondence: Dr Luis Cunha, Centre for Functional Ecology, Associate Laboratory  
20   TERRA, Department of Life Sciences, University of Coimbra, Coimbra, Portugal. email:  
21   luis.cunha@uc.pt

22 Abstract (250 words)

23 Earthworms thriving in naturally occurring geothermal soils offer rare insight into rapid  
24 adaptation to environmental extremes. Here, we show that the pantropical earthworm  
25 *Amyntas gracilis* survives and flourishes in soils of the Furnas Volcano (São Miguel Island,  
26 Azores), where conditions include elevated temperatures (up to 40°C), high CO<sub>2</sub> (88.6%),  
27 low O<sub>2</sub> (10%), toxic metals, and mildly acidic pH. In a reciprocal-transplant,  
28 mesocosm-based experiment between soils overlying areas of active degassing volcanic  
29 gassing (hereafter active degassing soils) and reference soils, convergence of the epidermal  
30 thickness of the transplanted earthworms to the resident-soil phenotype (24 ± 3.9 µm active  
31 degassing soil, 43.8 ± 8 µm reference soil), was observed within 31 days.

32 Combining RNA-Seq, DNA (5-cytosine) methylation mapping, and microRNA profiling, this  
33 phenotypic change results from coordinated transcriptional and epigenetic reprogramming.  
34 While gene-body methylation occurred at ~98 % of loci, levels varied, and differentially  
35 methylated regions were enriched for genes with altered expression under volcanic stress.  
36 Multi-omics network analysis identified epithelial morphogenesis, circulatory system  
37 formation, and neural development as regulatory hubs, highlighted by a set of 41 epithelial-  
38 morphogenesis genes showing consistent methylation and miRNA patterns. Additional  
39 modules governing ion transport and signal transduction complemented the adaptive  
40 response.

41 Collectively these findings demonstrate that *A. gracilis* employs dynamic DNA methylation  
42 and microRNA regulation alongside transcriptional reprogramming to generate a persistent  
43 phenotypic adjustment to a volcanic stress. This work advances our understanding of  
44 extremophile resilience and provides a scalable model for predicting organismal adaptive  
45 capacity in the face of environmental extremes.

46 Keywords: phenotypic plasticity, soil invertebrates, epigenetic regulation, adaptation,  
47 extreme environment

48

49

50 [Introduction](#)

51 Animals and plants living in extreme environments are frequently exposed to a diverse range  
52 of stressors, often at varying intensities. To survive, these species evolve integrated suites of  
53 anatomical, biochemical, physiological, and behavioural adaptations. Among soil-dwelling  
54 invertebrates, characterised by low dispersal and sedentary lifestyles, adaptive plasticity to  
55 environmental extremes is especially critical. Earthworms have been shown to adapt to  
56 metal pollution (Langdon, et al. 2003; Anderson, et al. 2017; Huang, et al. 2023), high  
57 altitude (Perry, et al. 2022), and floodwater inundation (Klok, et al. 2006). However, the case  
58 of the ability of the earthworm *Amyntas gracilis* to survive in soils affected by underlying  
59 volcanic activity is one particularly striking case (Cunha, et al. 2011; Cunha, et al. 2014),  
60 because this species must withstand a combination of high CO<sub>2</sub> flux (hypercapnia),  
61 temperature extremes, low O<sub>2</sub> (hypoxia), acidic pH, and elevated metal concentrations.

62 Organisms deploy a suite of conserved biochemical pathways (e.g., heat-shock proteins,  
63 metallothioneins, antioxidant enzymes, DNA methylation, and small RNAs) to mount plastic  
64 responses to stressors (e.g., (Lindquist and Craig 1988; Morgan, et al. 2007; Zhao, et al.  
65 2016; Wang, et al. 2021). In particular, cell-signalling cascades triggered by oxidative or  
66 osmotic imbalance illustrate how rapidly physiology can be reshaped in response to change  
67 (Martindale and Holbrook 2002; Wang, et al. 2020). Because these physiological shifts  
68 depend on coordinated changes in gene expression, organisms must couple environmental  
69 sensing to durable, yet flexible, regulatory systems. Thus beyond the immediate response,  
70 epigenetic marks (especially 5-methylcytosine) and non-coding RNAs (notably microRNAs)  
71 establish a heritable “regulatory memory” that can mediate non-Mendelian transmission of  
72 adaptive phenotypes across sub-Darwinian timescales (Schachtman and Goodger 2008;  
73 Geeleher, et al. 2012; Liebers, et al. 2014).

74 Earthworms are central to global food production as critical ecosystem service providers,  
75 modulating nutrient cycling, soil structure, and plant productivity (Fonte, et al. 2023).  
76 Understanding the molecular mechanisms underpinning their adaptive plasticity not only  
77 enables us to pinpoint species or populations capable of withstanding increasing  
78 environmental extremes but also offers a framework for assessing environmental stressor  
79 impacts across soil communities. In this study, we therefore focused on defining the  
80 underlying gene expression landscapes and two extra-genomic regulators, microRNA  
81 abundance and DNA (5-cytosine) methylation, to test their contributions to plasticity in the  
82 invasive earthworm *Amyntas gracilis*, following transplantation between soils effected by  
83 geothermally “degassing” and reference soils on São Miguel Island.

84 On the mid-Atlantic island of São Miguel, diffuse degassing affected volcanic soils, such as  
85 those in the Furnas area used for this study, are typified by soil temperatures up to 98°C and  
86 CO<sub>2</sub> degassing leading to soil CO<sub>2</sub> up to 100% leading to potential hypoxia or hypercapnia  
87 (Viveiros, et al. 2010; Viveiros, et al. 2015). Furthermore, these soils also contain elevated  
88 concentrations of the metals Cu, Pb, and Zn (Cunha, et al. 2011). Given these extreme  
89 conditions, it is surprising that soils in the Furnas Volcano area are colonised by three  
90 peregrine earthworm species, *Pontoscolex corethrurus* (Family: Rhinodrilidae) from South  
91 America, and *Amyntas gracilis* and *Amyntas corticis* (Family: Megascolecidae) from Asia  
92 while native European lumbricids, though widespread elsewhere on the island (Talavera, et  
93 al. 2020), are absent from the hydrothermal and degassing zone (Novo, et al. 2015).

94 The extremophile nature of *A. gracilis* was investigated by examining the suite of traits that  
95 enable this species to cope with the volcanism-linked stressors encountered in the Furnas  
96 area. It was hypothesised that *A. gracilis* possesses both genetically determined  
97 ("constitutive") traits and traits induced by plasticity. Previously, it was shown that the  
98 epidermis of degassing-site *A. gracilis* residents is significantly thinner than that of  
99 counterparts from non-degassing regions on São Miguel (Cunha, et al. 2014). This  
100 anatomical modification of the gas-permeable surface has been hypothesised to represent a  
101 plastic response that reduces diffusion distances and increases gas-exchange efficiency  
102 under prevailing anoxic conditions. In the present study, the regulatory molecular  
103 mechanisms governing this developmental change and physiological response were  
104 investigated. Three tiers of environmental response were quantified using a  
105 reciprocal-transplant, mesocosm-based design: (1) the immediate stress response to altered  
106 soil conditions, (2) genome-wide transcriptional changes, assessed by RNA-Seq, and (3) the  
107 extra-genomic regulatory mechanisms, microRNA abundance and DNA (5-cytosine)  
108 methylation, thought to orchestrate this adaptive plasticity. By integrating transcriptomic,  
109 methylation patterns, and small-RNA profiling, the reshaping of gene networks and the  
110 establishment of heritable regulatory states in *Amyntas gracilis* under geothermal versus  
111 reference soil regimes were elucidated.

112 Materials and Methods

113 The Azores archipelago comprises nine volcanic islands in the North Atlantic Ocean,  
114 between 36°45'–39°43'N and 24°45'–31°17'W, at the triple junction of the Eurasian, Nubian  
115 and North American plates. Due to this geodynamic setting, seismic and volcanic  
116 phenomena are common (e.g., Gaspar et al. 2015). São Miguel is the largest (757 km<sup>2</sup>) of  
117 the nine islands and is located in the eastern part of the archipelago. Across São Miguel,  
118 several manifestations of volcanism, including hydrothermal fumarolic fields, cold CO<sub>2</sub>-rich  
119 and hot thermal springs, as well as diffuse soil affected degassing sites, are present  
120 (Viveiros, et al. 2008; Viveiros, et al. 2010). To assess how earthworms respond to the range  
121 of normal to extreme soil conditions present on São Miguel, two field sites, differing in their  
122 degassing activity (e.g., with or without thermal and CO<sub>2</sub> degassing anomalies (with a  
123 maximum temperature of 47.3°C and a maximum CO<sub>2</sub> of 96.5% at 50 cm depth), were  
124 selected for a transplant experiment: (a) degassing sites located inside Furnas Volcano  
125 caldera (site referred to hereafter as “Furnas”), in the vicinity of the Furnas Village  
126 Fumarolic Field, a region that corresponds to an area of anomalous CO<sub>2</sub> degassing and  
127 temperature, and (b) a non-degassing site at the western flank of Fogo Volcano, at Chã da  
128 Macela (site referred to hereafter as “Macela”); although located on an active volcano,  
129 experience no recognised anomalous degassing or thermal anomaly (Ferreira, et al. 2005;  
130 Viveiros, et al. 2023).

131 Clitellate adult *Amyntas gracilis* were collected from a site in both the volcanic Furnas site  
132 (degassing earthworm collection site), 37° 46' 12" N 25° 18' 14.399" W and volcanic non-  
133 degassing site Macela (non-degassing earthworm collection site) 37° 45' 50.76" N, 25° 32'  
134 3.516" W by digging and hand-sorting. Collected individuals were randomly assigned to  
135 treatment replicates in a reciprocal, factorial transplant experiment, with earthworm origin  
136 and soil exposure location as experimental factors (Fig. 1a). Twenty-four hours after  
137 collection, earthworms were exposed either to degassing soil (hereafter “V”) from a grass-  
138 covered site in the Furnas caldera (37° 46' 22.8" N, 25° 18' 14.399" W), or to non-degassing  
139 reference soil (hereafter “M”) from a pasture near the Macela site (37° 45' 52.02" N, 25° 31'  
140 30.575" W). For each treatment replicate, ten individuals were weighed and placed into  
141 perforated, cube-shaped mesh bags (12 L volume) filled with local soil. Six replicate  
142 mesocosms per origin (Furnas or Macela) were placed at each exposure site (V or M),  
143 resulting in four treatments: VV (Furnas-origin in Furnas soil), VM (Furnas-origin in Macela  
144 soil), MM (Macela-origin in Macela soil), and MV (Macela-origin in Furnas soil) (Fig. 1b).  
145 Mesocosms were installed flush with the soil surface, ensuring continuous contact between  
146 soil and mesh for unhindered gas and pore water exchange. They were covered with a  
147 waterproof fabric to prevent waterlogging during heavy rainfall and to reduce moisture loss in

148 dry periods. Mesocosms were maintained in situ for 31 days. At the end of the exposure  
149 period, mesocosms were removed and earthworms were hand-sorted, survival recorded,  
150 and individuals reweighed. Three individuals per mesocosm were flash-frozen in liquid  
151 nitrogen for molecular analyses; the remaining specimens were transferred to the laboratory  
152 for further processing.

153

154 **Environmental characterisation**

155 Soil CO<sub>2</sub> flux measurements were performed with a portable soil CO<sub>2</sub> flux station (West  
156 Systems S.r.L., Pontedera, Italy) based on the accumulation chamber method (Chiodini, et  
157 al. 1998). Soil CO<sub>2</sub> and O<sub>2</sub> measurements were performed at the soil surface before starting  
158 the experiment following the methodology of Baubron et al. (1991) and gases further  
159 sampled at 25 and 50 cm depth using a GA2000 infrared gas detector (Geotechnical  
160 Instruments). Even if other volatiles (H<sub>2</sub>S, He, CO, Hg, <sup>222</sup>Rn) can be released in these  
161 environments, CO<sub>2</sub> represents the main volcanic gas released to these soils (Viveiros, et al.  
162 2010; Silva, et al. 2015; Bagnato, et al. 2018). Soil temperature was measured at the same  
163 depths as gas was sampled with a portable T51 Rotronic thermometer. The soil  
164 temperature, CO<sub>2</sub> and O<sub>2</sub> concentration measurements were performed before the setup  
165 and at the end of the experiment inside the mesocosm units.

166 To characterise soil physicochemical properties, samples were taken from each mesocosm,  
167 air-dried, and sieved at 2 mm. The soils were oven-dried for moisture determination at 105  
168 °C. Water-holding capacity was measured following ISO guideline 11274. Organic matter  
169 content was measured as loss on ignition at 500 °C in a muffle furnace (Rowell 1994). Soil  
170 pH was measured in suspensions of 10 g air-dried soil in 25 ml deionised water following  
171 shaking for 15 minutes (ISO 2005). Texture was calculated from the percentage of soil  
172 particles in the size ranges < 2 mm, 2 – 63 mm and > 63 mm as determined using a Malvern  
173 MasterSizer 200 with a Hydro2000MU wet dispersion unit. A sample of ~1.5 g of air-dried,  
174 sieved soil was analysed with an obscuration of 5 and 25 %. Instrument performance was  
175 checked using a Malvern 15- 150 mm quality audit standard and “general purpose sand, 40  
176 – 100 mesh” (Fisher Scientific, Loughborough, UK). Total concentrations of Al, Cr, Cu, Fe,  
177 Mn, Ni, Pb, Sr, Ti, and Zn were determined in a 1 g sample of the air-dried soil following  
178 *aqua regia* digestion (Arnold, et al. 2008). The certified reference material BCR-143R  
179 (Commission of the European Communities, Community Bureau of Reference) was also  
180 digested. Digests and method blanks were analysed by inductively coupled plasma-optical  
181 emission spectrometry (ICP-OES). Method blanks for Zn were above detection and results  
182 were blank corrected, for the other elements method blanks were below detection. Accuracy,

183 as assessed by comparison with the CRM was as follows: Al 127%, Cr 103%, Cu 94%, Fe  
184 104%, Mn 105%, Ni 90%, Pb 110%, Sr 104%, Zn 96%, Ti concentrations were not certified  
185 in the CRM.

186

#### 187 Metal body burden by subcellular fractionation

188 Six earthworms per treatment, one from each replicate for each of the four treatments (total  
189 n=24), were selected randomly and depurated for 36h on filter paper before freezing and  
190 fractionation (Arnold and Hodson 2007). The frozen earthworms were defrosted, weighed,  
191 homogenised in 0.01M Tris-HCl pH 7.5 and fractionated (Arnold et al., 2008) into three  
192 different subcellular fractions: a soluble fraction (SOL, comprising the aqueous and cytosolic  
193 fraction including soluble proteins such as metallothionein-like and heat-sensitive proteins).  
194 an insoluble fraction (MRG comprising metal-rich granules) and a second insoluble fractions  
195 (INT, tissue fragments, cell membranes and mitochondria/organelles). Individual fractions  
196 were digested in HNO<sub>3</sub> (Morgan and Morgan 1990), made up to volume with ultrapure water  
197 and analysed for the same metals as the soils but by inductively coupled plasma-mass  
198 spectrometry, together with As, Bi and Cd. The resulting concentrations are expressed as  
199 mg/kg (dry weight) of earthworm tissue.

200

#### 201 Genotyping

202 All earthworms used were genotyped using the cytochrome oxidase subunit I (COI) gene to  
203 confirm their species identity and avoid heterogeneity in the genetic background. Total  
204 genomic DNA was extracted from ~25 mg of tissue from the posterior section or  
205 cryogenically powdered tissue. DNAeasy Tissue Kit (Qiagen, Manchester, UK) was used  
206 with a final elution with two volumes of 70 µl of TE buffer. A segment of the COI gene was  
207 amplified using the primers LCO1490 and HCO2198 (Folmer, et al. 1994). Reactions  
208 contained: 4 µl of PCR buffer (Promega, Madison, Wisconsin), 2 µl of 25 mM MgCl<sub>2</sub>  
209 (Promega), 1 µl of 10mM dNTPs, 1 µl of each 10 µM primer, 1 U of Taq DNA polymerase  
210 (Promega), 1 µl of genomic DNA template, and sterile H<sub>2</sub>O to a final volume of 20 µl. The  
211 PCR profile was 94°C (5 min), 35 cycles of 94°C (30 s), 52°C (30 s), and 72°C (1 min), with a  
212 final extension of 10 min at 72°C. PCR products were purified and sequenced by Eurofins  
213 ([www.eurofinsgenomics.eu](http://www.eurofinsgenomics.eu)) using the same primers. Resulting COI sequences were aligned  
214 and compared against reference haplotypes from Novo et al. (2015) to confirm species  
215 identity and assess genetic uniformity prior to downstream omics analyses.

216

217 **Histological processing and morphometry**

218 Two surviving earthworms from each bag (total n=48) collected after 31 days exposure were  
219 depurated for 36 h on damp filter paper to allow them to egest the soil in their gut. The  
220 anterior parts (extending three segments posterior to the clitellum) of the purged earthworms  
221 were fixed in 4% formaldehyde buffered to pH 7 and stabilized with methanol, dehydrated in  
222 a graded ethanol series, cleared in xylene and infiltrated with paraffin wax in a Leica TP1020  
223 (Leica Microsystems, Wetzlar, Germany). The paraffin embedded samples were shaped into  
224 histological blocks ensuring the same sample orientation using a Leica Histocentre EG1150  
225 (Leica Microsystems, Wetzlar, Germany). Histological sections (4 µm thickness) were cut on  
226 a Leica Rotary microtome RM2035 (Leica Microsystems, Wetzlar, Germany), mounted on  
227 albumin-coated slides (Menzel-Glaser, Braunschweig, Germany) and dried at 40°C for 24 h.  
228 The slides were then stained with Alcian Blue (Ph 2.5)/ Periodic Acid Schiff (AB/PAS)  
229 (Banchroft, et al. 1996). Epidermis thickness of each earthworm was measured in 3 sections  
230 (4 fields per section), 40 µm apart. Images were captured using a CoolSNAP-cf camera  
231 (Photometrics GmbH, Munich, Germany) coupled to a light microscope Leica DM1000  
232 (Leica Microsystems, Wetzlar, Germany), and analysed with Image Pro-Plus 5.0 (Media  
233 Cybernetics, Silver Springs, Maryland). For statistics, the average value from 12  
234 measurements per individual was used for 12 earthworms per treatment. Epidermal  
235 thickness measurements were analysed (with or without log<sub>e</sub> transformation) by two-way  
236 ANOVA, with earthworm origin and exposure location as factors, with p≤ 0.05 taken as  
237 significant.

238

239 **DNA Methylation Immunoprecipitation, RNAseq and miRNA Library Preparation,  
240 Sequencing**

241 For Next Generation Sequencing analyses, we selected three replicate mesocosms (bags)  
242 out of the six per treatment and used the three previously flash-frozen earthworms from each  
243 to be powdered individually (whole body) by pestle and mortar under liquid nitrogen (total  
244 n=36). For total RNA extraction, ca. 50 mg of the powder was homogenised in 1.5 ml of  
245 Trizol (Life Technologies). After centrifugation at 12,000 g for 5 min, the supernatant was  
246 transferred to an Eppendorf and 240 µl of chloroform was added and the mix was incubated  
247 for 3 min. The sample was centrifuged at 12,000 g for 15 min (4°C), and the upper phase  
248 was mixed with 250 µl absolute ethanol. RNeasy mini columns (Qiagen) were used to clean  
249 the RNA, and samples were eluted by centrifugation at 8,000 g in two volumes of 30 µl of  
250 H<sub>2</sub>O. Extracted RNA quality, integrity and quantity were checked in a 2100 Bioanalyzer  
251 (Agilent) (RNA Nano Chip) and Nanodrop (Thermo Fisher Scientific). Twelve samples (three

252 replicates each comprising pooled RNA from three individuals from the same bag for each of  
253 the four transplant conditions) were poly-A selected and prepared for Truseq RNA paired-  
254 end cDNA library construction by Edinburgh Genomics ([genomics.ed.ac.uk](http://genomics.ed.ac.uk)). 100 bp paired-  
255 end libraries were multiplexed and sequenced in two Illumina Hiseq 2000 lanes (Illumina  
256 Inc).

257 Small RNAs were extracted from the same samples (36 samples pooled in 12 libraries)  
258 with miRNeasy Mini kit (Qiagen Ltd) following the manufacturer's guidelines. The samples  
259 were quality assessed using Bioanalyzer and Nanodrop and supplied to Edinburgh  
260 Genomics ([genomics.ed.ac.uk](http://genomics.ed.ac.uk)), where the libraries were prepared using TruSeq Small RNA  
261 library kit (Illumina Inc) and 50 bp single-end sequencing on an Illumina 2500 HiSeq platform  
262 using HiSeq V3 chemistry (Illumina Inc).

263 For the DNA methylation analysis, genomic DNA was extracted from powdered tissue using  
264 the same samples as for total RNA and small RNA using the DNeasy kit (Qiagen Ltd). DNA  
265 quality was assessed using a nanodrop spectrophotometer (Thermo Fisher Scientific), with  
266 integrity and size being determined using a 0.4% agarose gel electrophoresis. For each  
267 treatment, equimolar DNA aliquots from three individuals of a single replicate mesh bag, the  
268 same as those used in the RNA-Seq workflow, were pooled to ensure sufficient input.  
269 Libraries for MeDIP-Seq libraries were constructed following methylated-DNA  
270 immunoprecipitation using the DNA Methylation IP Kit (Zymo Research, Orange, CA).  
271 Briefly, pooled DNA was sonicated to ~200–500 bp fragments, denatured, and incubated  
272 with 5-methylcytosine-specific antibodies. Immunoprecipitated DNA was recovered, then  
273 subjected to a three-step PCR enrichment: first with primers containing partial adapter  
274 sequences and four random nucleotides to minimise bias, followed by two successive  
275 rounds of amplification to append full-length sequencing adapters and unique barcodes.  
276 Libraries were quantified using the Agilent 2200 TapeStation and by qPCR. Sample  
277 concentrations were normalised to 4 nM, before sequencing on an Illumina HiSeq 2500  
278 using 100 bp paired-end reads.

279

## 280 Generating the *A. gracilis* Genome

281 High-molecular-weight genomic DNA was extracted from a single adult *Amyntas gracilis*  
282 collected at the Furnas degassing site using a standard phenol–chloroform protocol. DNA  
283 quality was assessed by 1% agarose gel electrophoresis and quantified using a NanoDrop  
284 spectrophotometer (Thermo Fisher Scientific). A draft genome was subsequently generated  
285 using four paired-end libraries (insert sizes: 350 bp and 650 bp) and two mate-pair libraries  
286 (5 kb and 10 kb inserts), sequenced on an Illumina HiSeq 2500 platform. This yielded  
287 approximately 100x coverage with 150 bp paired-end reads and an additional ~10x

288 coverage from mate-pair libraries, with sequencing depth balanced across library types. K-  
289 mer analysis (Simao, et al. 2015) indicated a high level of heterozygosity, prompting the use  
290 of *Platanus* v1.2.4 for de novo assembly (Kajitani, et al. 2014). The initial graph-based  
291 assembly resolved allelic variation by collapsing bubbles representing heterozygous loci.  
292 Mate-pair reads were then employed during scaffolding to bridge repetitive regions and  
293 connect contigs. Finally, a post-assembly allelic-variant collapse step was performed to  
294 reduce redundancy, consolidating residual haplotigs into single consensus scaffolds,  
295 resulting in a high-quality haploid representation of the *A. gracilis* genome.

296

#### 297 Sequence Read Mapping Against the Newly Generated Genome

298 Short-read libraries for all three sequencing experiments were end-clipped and filtered with  
299 Trimmomatic (Bolger, et al. 2014). The RNASeq and Me-DIP libraries were aligned to the  
300 generated *A. gracilis* genome using BBmap (Bushnell 2014) with the pre-set ‘slow’. RNASeq  
301 libraries aligned to the genome at a mean rate of 86.1%, and the MeDIP libraries aligned at  
302 90.5% (see supplementary table S1 for library sizes and alignment rates). SAMtools was  
303 used to convert output SAM files to sorted and indexed BAM files (Li, et al. 2009). The  
304 ‘htseq-count’ function of the HTSeq python package was used to generate RNASeq data-set  
305 read counts. SAMtools (Li, et al. 2009) ‘bedcov’ was used to quantify MeDIP read-count  
306 levels within genes and promotor regions. Promotor/TS-factor motif binding levels were  
307 divided into two regions: 100 bp 5' of the transcription start site and 1 Kb 5' of the  
308 transcription start site. These read counts were not used for absolute methylation analysis  
309 and did not require normalisation.

310 Novel miRNA prediction was performed using MiRDeep2 (Friedländer, et al. 2012).  
311 Processed reads were aligned to the genome and collapsed into a non-redundant set with  
312 the mapper.pl script. The alignments were converted to novel mature miRNA predictions  
313 with the miRDeep2.pl script. A bowtie database (Langmead, et al. 2009) was built using a  
314 combination of the predicted miRNAs and the latest version of the MiRbase database  
315 (Griffiths-Jones, et al. 2006; Griffiths-Jones, et al. 2008). Bowtie was used to map the  
316 collapsed reads onto the database using default short read settings, and a custom script was  
317 used to extract the raw read counts per miRNA from the output. While our approach  
318 diverges from the MirDeep2 processing steps, generating non-normalized miRNA count data  
319 was necessary. This ensured a consistent input format for DESeq2, thereby maintaining the  
320 uniformity of the statistical pipeline and facilitating reliable downstream comparisons.

321 Studies in humans and *Drosophila* have discovered canonical cohorts of 1,917 and 258  
322 active miRNAs, respectively, according to miRbase (Kozomara, et al. 2019). The outputs

323 from this processing pipeline included upwards of 20,000 hits per sample. However, the read  
324 counts per hit exhibited a power law distribution, with 10,313 miRNA targets achieving an  
325 average read count of less than 20. To select the hits most likely to represent active  
326 miRNAs, and with reference to typical miRNA cohort sizes, the output set was limited to the  
327 top 2,000 hits by mean expression. All the novel miRNAs also fell within this upper range.  
328

### 329 Methylome Gene Models

330 Custom software called Renoo (<https://github.com/OliverCardiff/Renoo>) was developed to  
331 build methylation gene models for the MeDIP data set. This software reads SAM formatted  
332 alignment files and analyses the coverages of genomic annotation elements across  
333 normalised spatial intervals. These magnitudes within these intervals are then scaled by a  
334 coupling-vector to compensate for CpG density precipitation efficiencies (Wilson and Beck  
335 2016). The coupling vector was defined as the mean observed coverage per sample, divided  
336 by the all-sample mean. The tool developed also aggregates the MeDIP read coverage over  
337 a set of elementary annotations. For example, the 0-10%, 10-20% ... 90-100% intervals  
338 along the 5'->3' length of an exon. The scaled read pileup allows for the profiling of a typical  
339 coverage pattern over the set of all spatial element. The software also supports rank-  
340 grouping these intervals by an additional variable, in this case, global-average gene  
341 expression levels from the corresponding RNA-Seq libraries were used. This process  
342 involves sorting the elements into deciles of their parent gene's all-sample geometric mean  
343 expression level and calculating the Me-DIP read coverage intra-group arithmetic means per  
344 interval (see Fig. 2a).

345 Because our samples consisted of pooled tissues, where methylation can be highly  
346 cell-type-specific (Maegawa, et al. 2010; Lokk, et al. 2014), a binary-coverage model was  
347 implemented to estimate the probability of methylation occurrence. In this second pass,  
348 window read depths were converted to a presence/absence score, and the frequency of  
349 windows with nonzero coverage was reported (e.g., a 0.2 frequency indicates that 20 % of  
350 loci in that window exhibited any MeDIP-Seq signal).

351 To visualize methylation patterns in a unified framework, we constructed “methylation  
352 gene-models” composed of the following ordered features: a 34 bp proximal promoter, 5'  
353 UTR, three coding exons (separated by two introns), 3' UTR, and a 300 bp downstream  
354 flanking region. Individual genes lacking one or more annotations were coerced into this  
355 template, enabling direct comparison of methylation profiles across heterogeneous gene  
356 structures.

357

358 Differential Expression and Methylation Analyses

359 All differential expression comparisons were conducted using the same DESeq2 pipeline  
360 (Love, et al. 2014). The “normal” fold-change shrinkage estimator was applied to maximize  
361 stringency and reduce noise from lowly expressed features. This conservative approach was  
362 especially important for the more heterogeneous MeDIP-Seq libraries (see supplementary  
363 Fig. S1–S3 for count-versus-fold-change and significance plots).

364 The experimental design (Fig. 1b) defined five key contrasts. For RNA-Seq and miRNA-Seq,  
365 three adaptive-response scenarios were tested by comparing two groups of three libraries  
366 each: (1) Static vs Change, which evaluates environmental change detection by contrasting  
367 earthworms remaining in their native soil (non-degassing soil, MM; degassing soil, VV)  
368 against those transplanted to the opposite soil, MV and VM; (2) Origin vs Origin, which  
369 probes persistent, origin-specific signatures by comparing all degassing-origin earthworms  
370 (regardless of soil, VM, VV) against all non-degassing-origin earthworms (MM, MV); and (3)  
371 Destination vs Destination, which assesses acclimation by contrasting all earthworms  
372 residing in degassing soil (MV, VV) against those in non-degassing soil (MM, VM). For  
373 MeDIP-Seq, the four libraries supported two transplant-specific contrasts: (4) degassing-  
374 origin earthworms moved to non-degassing soil (VM) versus degassing earthworms  
375 maintained in degassing soil (VV), and (5) non-degassing-origin earthworms moved to  
376 degassing soil (MV) versus non-degassing earthworms maintained in non-degassing soil  
377 (MM).

378 To explore miRNA-mediated regulation, the top 2,000 expressed miRNAs were aligned  
379 against the set of annotated transcripts, derived via TransDecoder utility scripts in the Trinity  
380 package (Haas, et al. 2013), using Bowtie 2 with parameters -k 500 --mp 2 -L 7. This  
381 configuration allows up to 500 alignments per miRNA, lowers the mismatch penalty to 2, and  
382 reduces the seed length to 7 (the empirically optimal minimum for perfect-match seed  
383 mapping of miRNAs; Lewis et al. (2005)), with no soft clipping. No reported alignment  
384 exceeded two mismatches. The resulting miRNA–gene network (supplementary Fig. S5 and  
385 S6) was then used to interpret primary regulatory impacts in the Destination vs Destination  
386 and Origin vs Origin comparisons (the Static vs Change contrast yielded too few significant  
387 miRNAs for meaningful network analysis). Finally, we propagated DESeq2’s significant fold-  
388 changes for functional enrichment clustering through this network to generate gene lists  
389 representing the putative downstream targets of miRNA regulation.

390

391 **Functional Enrichment**

392 The functional profiles of differentially expressed genes were assessed using the DAVID  
393 web server (Huang, et al. 2007). The genes described in *A. gracilis* are not part of a  
394 standardised gene naming ontology, as this earthworm is novel with respect to '*omic*'  
395 analysis. A proteome was translated from a genome-derived transcriptome with  
396 Transdecoder (Haas, et al. 2013). This proteome was used to search the Uniprot/Swissprot  
397 database with 'blastp' (Camacho, et al. 2009). All hits achieving an e-value below 5e-05  
398 were retained and used as a symbol translation table for DAVID. The complete list of gene  
399 annotations was also provided to the web server as a 'background' against which to  
400 measure enrichment.

401 A 3x3 matrix of enrichment analyses was conducted, corresponding to three data types  
402 (RNA-Seq, miRNA-Seq, MeDIP-Seq) and three experimental contrasts ("Static vs Change,"  
403 "Origin vs Origin," "Destination vs Destination"; Fig. 1d). For each contrast, gene lists were  
404 defined by symbol-translated features exhibiting shrinkage-corrected Wald p < 0.05; for  
405 miRNA-Seq, lists were derived by propagating significant miRNAs through the miRNA–gene  
406 interaction network to their immediate neighbour transcripts. To ensure consistency and  
407 comparability, initial clustering was performed at Gene Ontology Biological Process Level 4,  
408 and each resulting cluster was subsequently annotated for Cellular Component via simple  
409 enrichment. Fig. 1c shows the omics data sets generated: RNA-Seq (4 treatments x 3  
410 replicates), miRNA-Seq (4 x 3), and MeDIP-Seq (4 x 1 pooled replicate).

411 For the visualisations generated (Figs. 3–5), overlapping ontology terms were collapsed  
412 according to predefined rules: the more specific term was retained unless it overlapped at  
413 the same hierarchical depth, in which case the next most significant lower-level term was  
414 substituted. This procedure was intended to maximise descriptive resolution while preventing  
415 redundant labelling (e.g., "transmembrane ion channel" was not redundantly labelled as both  
416 an ion channel and a membrane protein).

417 Finally, to produce a unified representation of enriched functions, clusters sharing the same  
418 representative GO term across all three contrasts and data types were merged. For  
419 example, an "Epithelial Development" trait was defined by the union of all gene lists from  
420 clusters containing GO:0060429, with the most significant p-value per cluster being retained.

421 Results

422 Environmental and Soil Physicochemical Parameters at Degassing and Reference Sites

423 supplementary table S2 shows the gas and temperature conditions for soils at the degassing  
424 (Furnas) and non-degassing (Macela) sites. The mean temperature at a depth of 25 cm  
425 measured prior to mesocosm placement was 37 °C (with a minimum of 29.8 and a maximum  
426 of 47.3 °C) in the degassing affected transplant site soil, compared to 18°C (with a minimum  
427 of 17.8 °C and a maximum of 19.3 °C) for the degassing affected earthworm collection site  
428 soil and 17 °C (with a minimum of 16.2 °C and a maximum of 17.6 °C) at the non-degassing  
429 site soil. The CO<sub>2</sub> mean volume was 48.6% (with values between 14% and 96.5%) for the  
430 degassing transplantation soil, compared to 6.9% (with a min. of 14% to a max. 96.5%) at  
431 the degassing earthworm collecting site and 0.7-0.8% at the non-degassing collection and  
432 transplantation sites. The mean O<sub>2</sub> % (~10%) was consistent between the degassing  
433 transplant site and the degassing earthworm collection site soils. O<sub>2</sub> levels were higher in the  
434 non-degassing site collection and transplant site soils (~18%), indicating a potential for  
435 hypoxia and hypercapnia in soils of the volcanic degassing site.

436 Soil physical properties indicated differences between the degassing and non-degassing  
437 locations, but not between the degassing transplantation and earthworm collection  
438 degassing site soils (supplementary table S3). The degassing site soils had a reduced water  
439 holding capacity, approximately 50% lower clay content, and a higher sand content than the  
440 non-degassing site soils. Degassing soils also had <50% of the organic matter content of the  
441 Macela soils (~11% vs ~25-35%). Soils at the Furnas degassing site had Pb (108 ±14  
442 mg/kg) and Cu (96 ± 12.1 mg/kg) concentrations ~6 and ~5 times higher than those at  
443 Macela site soils. Nickel levels at Macela (27.4 mg/kg) were ~3.5 times higher than in the  
444 degassing soils (Table 1). All site soils were mildly acidic (supplementary table S3). All four  
445 soil treatments are silt-dominated loams with very low clay content (<5%) and moderate  
446 sand (~35–50%), with lower silt and higher sand content in the V compared to M soil  
447 (supplementary table S3).

448

449 Earthworm Genotyping and Genome Assembly

450 Mitochondrial COI barcoding of sampled individuals revealed two haplotypes differing by a  
451 single nucleotide over 648 bp, consistent with previously described São Miguel *A. gracilis*  
452 lineages (Novo, et al. 2015), thereby confirming species identity and genetic uniformity prior  
453 to downstream omics analyses.

454 The generated genome assembly N50 was 478Kb, with 4,350 scaffolds, and a total  
455 reconstruction genome size of 589Mb. This genome is available at NCBI Bioproject  
456 PRJNA513445. The final gene model identification and annotation was created using

457 MAKER2 (Holt and Yandell 2011). In total, 26,951 gene models were predicted. The  
458 genome was 78% complete for Metazoan BUSCO genes (Simao, et al. 2015), with a  
459 duplication rate of 11%, a fragmented rate of 4.9%, and a missing rate of 16%. This  
460 assembly shows no evidence of allelic inflation and, therefore, likely represents a good  
461 haploid representation of the genome. A secondary version of the assembly shows a higher  
462 level of completeness indicated through an 87% BUSCO score, but a smaller N50 of 370 Kb.  
463 This assembly exhibited a 19% duplication rate, a feature that may indicate that not all loci  
464 have collapsed to their haploid counterparts. As such, this genome may contain unphased  
465 diploid copies of some genes. For completeness, this version is also available through NCBI  
466 Bioproject PRJNA513445.

467

#### 468 Earthworm Tissue Metal Concentrations

469 Earthworm metal burdens (Table 2) were overwhelmingly partitioned into the internal/tissue  
470 fraction (INT), with the soluble pool (SOL) carrying an intermediate load and the metal-rich  
471 granule fraction (MRG) the smallest. On average across treatments, INT held roughly 80–  
472 90% of the total body load of each metal, SOL about 5–15%, and MRG only 1–10%. Fe, Cu,  
473 Cd, and Pb all adhered to this INT >> SOL > MRG hierarchy (Tukey HSD p < 0.05). Granule-  
474 bound Al and Mn were significantly enriched compared to their soluble pools (Al: 400 mg/kg  
475 vs. 27 mg/kg; Mn: 14 mg/kg vs. 40 mg/kg in MRG and SOL respectively; Tukey HSD p <  
476 0.05), capturing a disproportionate proportion of these potentially reactive elements and  
477 thereby limiting their cytosolic availability. For example, Al in INT averaged ~2 500 mg/kg  
478 (VV), approximately 83% of the totalled concentration of Al, versus ~27 mg/kg in SOL (~1%)  
479 and ~400 mg/kg in MRG (~13%).

480 Absolute metal levels were significantly affected by treatment type with the distribution of  
481 metals between tissue fractions remaining consistent for each metal. Earthworms in  
482 degassing soils (VV, MV) accumulated significantly more total and soluble Cu, Cd, Pb, and  
483 Bi than those in non-degassing soils (VM, MM) (all pairwise p < 0.05). Total Cu, for instance,  
484 was over three times higher in VV and MV than in MM, and Cd and Pb in SOL increased by  
485 0.5 to 1 times higher under degassing conditions. Conversely, Ni was highest in Macela-  
486 exposed worms (VM, MM), with VM showing more than four times the Ni levels of VV (Tukey  
487 HSD p < 0.05), reflecting the elevated Ni content of Macela soils.

488

#### 489 Morphometric Changes

490 After 31 days in either the active degassing (V) or non-degassing (M) soils, earthworm  
491 epidermal thickness matched the resident soil conditions regardless of origin (supplementary  
492 Fig. S4). In degassing soils, mean epidermal thickness was  $24 \pm 3.9 \mu\text{m}$ , whereas in Macela

493 soils it was  $42.8 \pm 8 \mu\text{m}$ . Furnas-origin earthworms transplanted to Macela exhibited a 78.3  
494 % increase in epidermal thickness relative to V controls, and M-origin worms moved to V  
495 showed a 44.1 % decrease (Tukey HSD,  $p < 0.05$ ). Body-mass changes of the earthworm  
496 showed that those remaining in the active degassing V site soil lost 10.7 % of their initial  
497 mass, those remaining in M site soil lost 3.3 %, VM transplantees gained 5.4 %, and MV  
498 transplantees lost 13.6 % (supplementary Fig. S4).

499

#### 500 Methylome Models

501 Of the 26,951 genes analysed, 93.5 – 96.4% were gene-body methylated to some extent  
502 (100+ MeDIP reads mapped on average). Fig. 2a shows a visualisation of the consolidated  
503 MeDIP read mappings to the common static gene model of methylation read depth for  
504 genes. There are clear differences between the rates of read alignment per gene element.  
505 The separation in methylation rates occurs most strongly between the lowest five ranks'  
506 groups, indicating that the lower 50% of the gene expression ranks have a positive linear  
507 relationship between their epigenetic interactions and their expression level. In contrast the  
508 upper 50% of the group showed little correlation. These conclusions are supported by both  
509 the relative read depth and methylation probability models.

510 Overall, coding sequences were more likely to receive highly abundant MeDIP read mapping  
511 than promoter regions, with methylation more prominent in the centre of the gene model  
512 than towards the 5` end. However, a binary state comparison of the gene model  
513 demonstrates that more individual introns had a higher methylation probability than individual  
514 coding sequences (Fig. 2b). This suggests that exonic methylation occurs more abundantly  
515 and in more consistent locations, whilst intronic methylation occurs less frequently and in a  
516 more diverse set of loci. With some inter-sample variability, 9-12% of primary promoter  
517 regions are predicted to be methylated. Methylation probability in the binary model also  
518 highlighted that the most regularly methylated intragenic features (at any abundance) were  
519 the intronic splice junctions, with an overall rate of 28-34% of the full set of junctions  
520 methylated to some degree across the four samples in the gene model. This suggests these  
521 splice-junctions are the gene elements that most broadly interact with DNA methylation.

522

#### 523 miRNA Networks

524 An initial miRNA network was generated based on the set of identified miRNA-to-gene  
525 binding relationships. In total, 168 novel mature miRNAs were predicted. This network  
526 visualisation and edge-distribution summary are shown in Fig. 2c and 2d. Of the 26,951  
527 genes, 9,363 (34%) had at least one miRNA binding site on the conservative rule of two

528 base changes or less compared to the mature sequences. Of these, 8,026 (85.7%) genes  
529 were bound by one miRNA, with the rest binding multiple (Fig. 2d). For the 2,000 putative  
530 miRNAs included in the alignment query, 1,554 (77%) were indicated to bind to one or more  
531 genes, suggesting some degree of over-inclusion error given the arbitrary selection cut-off.  
532 Of these miRNAs, 623 (37.4%) only bound a single gene, the rest binding multiple genes,  
533 including a small number of highly connected genes (Fig. 2d). Since miRNA functional  
534 impact was assessed relative to the bound genes, unbound miRNAs were not included in  
535 the annotation enrichment group analysis.

536 For functional analysis, the abundances of p-significant genes related to miRNA changes in  
537 this, and later sections are gathered based on the p-significance of the binding miRNAs.  
538 Thus, the functional description of the miRNA networks involved in expression change  
539 between samples was performed based on gene, rather than miRNA, annotation. The  
540 obtained differential miRNA expression sub-networks are shown in supplementary Fig. S5  
541 and S6 for the “Origin vs Origin” and “Destination vs Destination” respectively, as the “Static  
542 vs Change” test did not yield enough p-significant results to generate a usable network. In  
543 both possible experimental comparisons, functional enrichment clustering of genes  
544 annotated by Gene Ontology BP4 in DAVID yielded similar sets of results to the clustering  
545 experiments for the other analyses. Both networks included a highly enriched proportion of  
546 membrane-bound proteins. Neural system development was featured in multiple highly  
547 abundant clusters in the “Origin vs Origin” test (Counts: 130, 46, 45, 11) and in two less  
548 abundant but still highly significant clusters in the “Destination vs Destination” test (Counts:  
549 31, 19). The “Destination vs Destination” network also showed a cluster of 27 ion channel-  
550 related genes and a significant gene cluster for vasculature development (Count: 20) and  
551 blood circulation (Count: 16). A cluster of 41 genes within the category “morphogenesis of an  
552 epithelium” was significant for “Origin vs Origin” test (supplementary Fig. S5).

553

#### 554 [Expression Pattern Assessment](#)

555 The most substantive expression pattern difference between sample groups was in the  
556 “Destination vs Destination” test (Fig. 1d). In this comparison, both the miRNAseq and  
557 RNAseq datasets showed a pattern of significant p-value counts differential with each  
558 treatment comparison (Fig. 1d and 1d). The greatest difference between the number of  
559 significant features between the miRNA and RNAseq datasets was for the “Origin vs Origin”  
560 case. For this comparison, a stronger signature of effects was evident for the miRNA dataset  
561 (middle panel Fig. 1d) compared to the RNAseq dataset (top panel Fig. 1d).

562 Methylation sample variance was consistently bigger than for the other two ‘omics datasets,  
563 likely linked to the lack of replication, use of whole-body tissue-derived DNA and potential  
564 method variations (supplementary Fig. S3). Despite this, a set of consistent changes in  
565 gene-body methylation in the experimental comparisons was found that showed an  
566 identifiable functional specificity as seen also for the RNAseq and miRNA datasets. Overall,  
567 the number of *p*-significant changes in the MeDIP data was broadly similar (~3,000) for the  
568 three comparisons, although the significant gene sets differed markedly. In the “Static vs  
569 Change” MeDIP comparison, the significant gene set generated functional cluster fold  
570 enrichment scores higher than for any other gene list (top panel Fig. 1e), including the other  
571 two methylation tests, as displayed by the DAVID Functional Clustering (Middle and Bottom  
572 panel Fig. 1e).

573

#### 574 **Functional analysis of changes in the RNA and DNA methylation datasets**

575 Enrichment cluster intersection maps in the right-hand portions of Fig. 3-5 show the most  
576 significant cluster terms per data source (RNAseq, miRNA, MeDIP). This network view  
577 enables comparison of enrichment effects on identical terms across data sources. Notably,  
578 every top term identified for a given data type overlaps with at least one enrichment cluster  
579 from another source (intersections labelled using the lowest *p*-value term). Furthermore,  
580 terms and clusters unique to a single data source are among the least enriched or  
581 significant.

582 Comparing between Fig. 3-5, the same intersections are identified, however enrichments  
583 and significances vary by data source. The top emergent cluster intersections are shown in  
584 Fig. 6 as a trait matrix. These merged clusters summarise the detailed patterns of effects  
585 within five main identified functional categories: 1. Circulatory system Development (GO:  
586 0072359); 2. Epithelial Development (GO: 0060429); 3. Ion Transport (GO:0006811); 4.  
587 Neuron Development (GO: 0048666); 5. Signal Transduction (GO: 0007165). The net  
588 up/down regulation of genes annotated with these terms along with the associated miRNA  
589 expression changes are also shown in the trait matrix. There is a consistent pattern by which  
590 more genes with significantly upregulated miRNAs were found in the first four functional  
591 categories for the “Destination vs Destination” test (lefthand column plots Fig. 6), whereas  
592 the same categories in the “Origin vs Origin” test show a net down-regulated miRNA-gene  
593 component (Middle column plots Fig. 6).

594 Reflecting the functional enrichment differences in the MeDIP-Seq tests, significant  
595 differential methylation was most common in the “Static vs Change” test for the functional  
596 categories: ‘ion transport’, ‘neuron development’ and ‘signal transduction’. In this test, more

597 genes were affected than in any other data source comparison (compare righthand column  
598 plots to lefthand and middle Fig. 6). Methylation significant change rates for the functional  
599 categories of ‘circulatory system development’ and ‘epithelial development’ were consistent  
600 across the comparisons, suggesting that these levels may be more reflective of a conserved  
601 function change identified out with the inherent noise in the dataset.

602

603 Discussion

604 Our multi-tiered analysis reveals how *Amyntas gracilis* orchestrates morphological,  
605 physiological, and molecular responses to thrive in volcanic environments. Reciprocal  
606 transplants between degassing V soils and reference M soils uncovered consistent patterns  
607 of metal handling, tissue remodelling, and multi-omics reprogramming that underpin this  
608 earthworm's remarkable plasticity.

609

610 The *Amyntas* Genome System and Its Contributions to Function

611 The assembled genome of the megascolecid earthworm *Amyntas gracilis* enables an  
612 unprecedented integrative analysis of its adaptive responses to extreme volcanic-soil  
613 conditions. Until now, studies of soil-invertebrate adaptation have primarily focused on either  
614 transcriptional changes alone (Bhambri, et al. 2018; Novo, et al. 2020) or on coarse,  
615 genome-wide assessments of DNA-methylation shifts (Sruti, et al. 2017; Newbold, et al.  
616 2019). By contrast, our work combines physiological, transcriptomic, miRNA, and  
617 DNA-methylation data to generate a holistic view of phenotypic plasticity and regulatory  
618 network remodelling under geothermal stress.

619 Consistent with prior invertebrate studies showing that methylation predominantly marks  
620 gene bodies and transposable elements (Mandrioli 2007; Suzuki, et al. 2007; Sarda, et al.  
621 2012) (Guynes, et al. 2024), we find that 95–98% of *A. gracilis* genes bear some level of  
622 methylation. However, our differential-methylation models reveal that promoter regions,  
623 although less heavily methylated overall, undergo disproportionately large methylation  
624 changes in response to environmental shifts. This suggests that in earthworms, as in other  
625 invertebrates, promoter methylation may act as a dynamic regulatory switch, even if it  
626 constitutes a minority of total marks. Up to now, divergence from vertebrates has been  
627 attributed to the absence of promoter methylation and higher levels of gene body  
628 methylation in invertebrates (Keller, et al. 2016).

629 Intronic splice-junctions exhibited particularly high methylation probabilities (28–34% of all  
630 junctions; Fig. 2b), hinting at a conserved, epigenetic role in alternative-splicing regulation. In  
631 vertebrates, methylation near exon–intron boundaries can modulate RNA-pol II kinetics and  
632 splicing-factor recruitment, e.g. by preventing CTCF binding and altering Pol II pausing to  
633 favour exon skipping (Shukla, et al. 2011) or by recruiting methyl-CpG-binding proteins that  
634 guide splicing regulators (Du, et al. 2015). Although our current RNA-Seq analysis  
635 addressed gene-level expression, future isoform-resolved studies (e.g. MeDIP-Seq  
636 combined with long-read RNA-Seq) could directly test whether junction methylation fine-  
637 tunes transcript diversity under volcanic stress, a heritable “splicing code” facilitating rapid  
638 adaptation.

639 Substantial inter-individual variability in gene-body methylation was observed across  
640 transplant treatments, mirroring the concept of variable methylation regions (VMRs) as  
641 facilitators of heritable phenotypic diversity around a mean trait value (Feinberg and Irizarry  
642 2010). Functional clustering of sites showing differential methylation, gene expression, and  
643 miRNA regulation consistently highlighted developmental and signalling pathways (e.g.,  
644 epithelial morphogenesis, circulatory-system development, neuronal differentiation, ion  
645 transport, and signal transduction). This concordance suggests that stochastic methylation  
646 changes not only introduce heritable phenotypic variation, but also selectively target  
647 conserved adaptive pathways, perhaps reflecting convergent epigenetic strategies across  
648 distant taxa (Alakarppa, et al. 2018; Klupczynska and Ratajczak 2021).

649 Individual miRNAs were found to bind dozens of targets, paralleling the extensive regulatory  
650 reach noted in mammals (Friedman, et al. 2009). A pronounced “origin effect” — defined as  
651 persistent molecular differences attributable to native-soil history — was observed in miRNA  
652 profiles, exceeding that seen in mRNA expression. In earthworms from degassing soils, a  
653 net reduction in miRNA abundance was recorded, which is expected to diminish  
654 post-transcriptional repression of adaptive genes and, thus, maintain an epigenetic  
655 “memory” of prior environmental exposure, potentially bolstering resilience under variable  
656 conditions.

657 The global action of miRNAs has been characterised as predominantly repressive (Cai, et al.  
658 2009; Bartel 2018). This repressive trend was recapitulated in our analyses of the Epithelial  
659 Development and Circulatory System Development pathways, where inverse correlations  
660 between net miRNA and net mRNA regulation were detected in both “Destination vs.  
661 Destination” and “Origin vs. Origin” comparisons. Specifically, miRNA levels were found to  
662 be upregulated in the “Destination vs. Destination” test and downregulated in the “Origin vs.  
663 Origin” test, implying that, during acute acclimatisation, miRNAs act chiefly to suppress their  
664 transcriptional targets. Conversely, the reduction of miRNA abundance in degassing-origin  
665 earthworms suggests that repression of adaptive trait-associated transcripts is selectively  
666 relieved, thereby preserving expressed phenotypes that may confer adaptive advantage in  
667 fluctuating environments.

#### 668 **Physiological acclimation and adaptation**

669 Pronounced epidermal remodelling was induced by soil transplantation, independent of  
670 earthworm origin. In previous work, earthworms maintained in degassing Furnas soils  
671 exhibited a thinned epidermis (~24 µm), whereas those in non-degassing Macela soils  
672 retained the resident-soil norm (~40 µm)(Cunha, et al. 2011). Such adjustments parallel  
673 morphotype changes documented in hydrothermal-vent polychaetes (Andersen, et al. 2006)

674 and are consistent with an adaptive response to high CO<sub>2</sub>, low O<sub>2</sub>, and elevated  
675 temperature. Transcriptomic analysis identified 181 genes in the epithelial-development  
676 pathway, with a >5 times enrichment, confirming the breadth and strength of the genetic  
677 program driving this morphological shift. Notably, this pathway was activated in both native  
678 and transplanted individuals, indicating true acclimatisation rather than tissue damage.  
679 Conversely, epidermal restructuring and cellular alterations in oligochaetes has been related  
680 to metal or drought stress and as a protection against desiccation and microbial invasion,  
681 demonstrating that abiotic challenges can bidirectionally modulate cuticle architecture  
682 (Cunha, et al. 2011; Wang, et al. 2011; Briones and Álvarez-Otero 2018; Kumari, et al.  
683 2024). Body-mass trajectories mirrored these barrier changes: VM transplants gained  
684 weight, suggesting metabolic relief (Daniel, et al. 1996), whereas MV transplant worms lost  
685 most weight, reflecting the higher physiological toll of survival in active degassing soils  
686 (supplementary Fig. S4). The rapid convergence of epidermal thickness on destination  
687 values underscores its utility as a sensitive, short-term bioindicator organism stress.

688 Epigenetic profiling and miRNA data further supported the centrality of epithelial  
689 restructuring as a response to volcanic extremes. In the “Static vs Change” comparison,  
690 transcript and miRNA pathway-level responses were neutral overall (Fig. 6), yet differential  
691 methylation within this same contrast yielded a tightly focused network of  
692 epithelial-morphogenesis genes (Fig. 3–5). This suggests that DNA methylation plays a  
693 targeted role in regulating barrier pathways. Comparable patterns in crayfish link gene-body  
694 methylation to expression stabilisation via chromatin remodelling (Jeltsch and Jurkowska  
695 2014; Gatzmann, et al. 2018), hinting that similar mechanisms may control  
696 transcription-factor access during epidermal adaptation in *A. gracilis*.

697 Although earthworms possess both a closed, haemoglobin-based vasculature for gas  
698 transport and an open, hydrostatic vascular network for locomotion (Rieger and Purschke  
699 2005; Reiber and McGaw 2009; Monahan-Earley, et al. 2013), GO annotations for  
700 circulatory system development may reflect shared evolutionary origins rather than discrete  
701 functional modules. Crucially, however, the epidermis itself plays a central role in cutaneous  
702 gas diffusion (Mendes and Nonato 1957), suggesting that genes driving vascular  
703 morphogenesis in our datasets may actually contribute to enhancing oxygen uptake and  
704 CO<sub>2</sub> release through the skin.

705 Merged-cluster analyses, differential expression, and DNA-methylation changes all implicate  
706 both angiogenic and morphogenic remodelling of the integument (Fig. 4 and 6). Notably, the  
707 number of RNA-seq significant genes in circulatory pathways differs markedly between  
708 “Origin vs Origin” and “Destination vs Destination” contrasts, indicating that vascular

709 restructuring is enacted as an active acclimation response rather than a fixed developmental  
710 trait. The “Static vs Change” test further reveals stochastic methylation variation on these  
711 same genes, highlighting DNA methylation’s role in fine-tuning circulatory remodelling under  
712 each O<sub>2</sub>/CO<sub>2</sub> regime.

713 Neuron development was the third morphogenic trait category highly enriched in all three  
714 comparisons, albeit in different ways. Changes in neural development can be viewed in  
715 conjunction with changes in the signal transduction annotation cluster, as the two overlap  
716 considerably via their constituent genes. Signal transduction is a very broad category and  
717 can be difficult to disaggregate. However, there was a clear pattern for neurogenesis-  
718 associated terms to comprise a substantial part of this subset. It has been shown that  
719 invertebrates such as *Drosophila melanogaster* possess dedicated O<sub>2</sub> and CO<sub>2</sub> neural or  
720 olfactory chemical signalling pathways (Luo, et al. 2009). Our results suggest that similar  
721 pathways may be triggering the morphometric changes seen in the epidermis and  
722 associated circulatory system. Further, hypoxia encountered by the volcanic site earthworms  
723 has been shown to substantially affect neural stem cell differentiation. Research has shown  
724 neuronal migration defects and axon pathfinding changes in *Caenorhabditis elegans* (Chang  
725 and Bargmann 2008), reducing ion concentrations and leading to hyper-polarization in *D.*  
726 *melanogaster* (Gu and Haddad, 1999) and cation co-transporter activity reduction and  
727 resultant hyper-polarization in *Lymnaea stagnalis* (Silverman-Gavrila, et al. 2009).

728 Most of the literature concerning neural responses to hypoxia in invertebrates concerns  
729 membrane-based changes, with little consideration of differentiation and growth alterations  
730 (Mannello, et al. 2011). This is reflected in Fig. 5 where the abundance of membrane-bound  
731 proteins in the miRNA-regulation network is displayed. A substantial number of neurogenic  
732 genes are also identified here, suggesting a role as a more general plasticity response.  
733 Signal transduction pathways were generally strongly differentially methylated in the “Static  
734 vs Change” test compared to any other comparisons. Neural development-specific pathways  
735 also nearly double the rate of differential methylation in this test. This suggests that the  
736 ‘general’ environmental change response exhibited may constitute the epigenetic  
737 modification of many of the same signalling pathways regardless of the specific nature of the  
738 transition encountered by the earthworms. Uniquely, the signal transduction merged cluster  
739 also showed more RNAseq differential significance in the “Static vs Change” test, indicating  
740 a more general change response.

741 **Metal Homeostasis via Compartmentalization and Molecular Drivers of Metal Detoxification**  
742 Across all treatments, earthworms partitioned metals consistently into three subcellular  
743 pools, INT > SOL > MRG, revealing an evolutionarily conserved sequestration strategy. The

744 INT fraction, encompassing tissue fragments, membranes, and organelles, likely reflects  
745 both the incorporation of essential metals into metabolic pathways and the non-specific  
746 adsorption of excess metals onto cellular structures. The SOL fraction acts as a dynamic  
747 buffer, modulating the immediate bioavailability of metals via soluble proteins, such as  
748 metallothioneins, and other cytosolic constituents (Höckner, et al. 2015; Swart, et al. 2022).  
749 Finally, the MRG pool provides a dedicated detoxification sink, especially prominent for Al  
750 and Mn, thereby shielding critical biomolecules from redox-driven or catalytic damage.

751 Treatment-specific shifts in metal burdens mirrored soil geochemistry without altering this  
752 hierarchy. In V soil exposed worms, soils enriched in Cu, Cd, Pb, and Bi drove elevated  
753 accumulation in both INT and SOL fractions. In contrast, earthworm kept in M soil showed  
754 pronounced Ni uptake, predominantly allocated to the INT compartment, transplants,  
755 reflecting site geochemistry. For As concentration were elevated especially for the MV  
756 treatment indicating that the transplanted earthworms failed to regulate internal  
757 concentration through mechanisms such as metallothionein binding or granular  
758 sequestration to the same extent site as native earthworms in the VV treatment. This  
759 observation is consistent with the known toxicity of As and prior reports of epigenetic  
760 disruption playing a role in these effects (Kille, et al. 2013). Indeed, that the methylation  
761 differentials for ion-transporter genes were markedly higher in the “Static vs Change”  
762 comparison, suggesting a broad-scale epigenetic response to prevailing exposure conditions  
763 linked to changes in metal trafficking requirements.

764 The distribution of metals across different cellular fractions suggests that intrinsic  
765 sequestration capacities, acting consistently at different exposure levels, govern earthworm  
766 resilience to metals. The conserved INT >> SOL > MRG partitioning defines a robust  
767 detoxification framework adaptable to diverse metal loads associated with soils impacted by  
768 volcanic degassing conditions and anthropogenic contamination. Key pathways involved in  
769 this response can be understood from our combined gene expression and epigenetic  
770 analyses

771 Differential omics analyses, including transcript expression, miRNA targeting, and DNA  
772 methylation mapping, identified an ion-transport annotation cluster of over 200 genes with  
773 significantly altered regulation. Notably, 36.4 percent of these genes encode metal-ion  
774 transporters, central to cellular metal homeostasis. Metallothioneins, small cysteine-rich  
775 proteins synthesized in the Golgi and likely localized within the SOL fraction, emerged as  
776 principal metal detoxification agents (Höckner, et al. 2015). Consistent with their established  
777 roles in Zn and Cd binding, SOL abundances of these metals in earthworms exposed to

778 degassing soils suggest metallothionein-mediated regulation, whereas Cu regulation via this  
779 mechanism is more nuanced in its response (Swart, et al. 2022).

780 Beyond Zn and Cd, Pb exhibited increased storage in the INT fraction of active degassing V  
781 soil exposed earthworms. For Pb this increase was especially noticeable, with this metal  
782 likely bound to phosphate-ligated granules in chloragogenous tissue in this fraction (Morgan  
783 and Morgan 1990). This site effect on metal levels is mirrored by a consistent set of miRNA  
784 interactions in both “Destination vs Destination” and “Origin vs Origin” comparisons,  
785 indicating coordinated post-transcriptional control.

786

787 While epidermal thinning under low-O<sub>2</sub>, high-CO<sub>2</sub> conditions appears to be a general plastic  
788 response among oligochaetes, *A. gracilis* ability to tolerate and even thrive in extremely  
789 elevated metal environments may define its success in V soils. Our integrated analyses  
790 show that *A. gracilis* combines constitutive expansions of detoxification gene families with  
791 highly plastic regulatory control of metal-handling pathways. Comparative genomic analyses  
792 of ion-transport and detoxification repertoires across co-occurring lumbricid and  
793 megascolecid species would clarify whether *A. gracilis* possesses uniquely enriched or more  
794 rapidly inducible metal-handling loci, and whether metal tolerance, rather than hypoxia  
795 alone, underpins its success in volcanic soils.

796

#### 797 Heat Exposure and Hypoxia-Driven Responses

798 Individual genes, particularly those encoding heat-shock proteins, chaperonins and other  
799 stress-induced factors, are well known to respond transcriptionally to elevated temperatures  
800 (e.g. Schoville, et al. 2012; Lockwood, et al. 2017). Similarly, the trehalose transporter Tret1-  
801 2, which mediates the accumulation of the relatively heat-stable disaccharide trehalose, is  
802 upregulated under combined temperature and drought stress (Lopienska-Biernat, et al.  
803 2019; Perez and Aron 2023). However, among the main group of annotation clusters, GO  
804 Terms linked to exposure to heat stress (e.g. GO:0031072: Heat shock protein binding;  
805 GO:0009408: Response to heat; GO:0034605: Cellular response to heat) were, perhaps  
806 surprisingly, not among the most enriched sets of pathways identified.

807 Despite extreme soil temperatures, >40°C in degassing sites, indicating potentially  
808 significant heat exposure that exceeds the thermal tolerance of many temperate earthworm  
809 species (Viljoen and Reinecke 1992; Edwards and Bohlen 1996). However, despite this  
810 evidence heat tolerance, *Amynthas gracilis* showed neither a canonical heat-shock response  
811 nor enrichment of GO terms such as GO:0031072 “Heat-shock protein binding,”

812 GO:0009408 “Response to heat,” or GO:0034605 “Cellular response to heat.” It should be  
813 noted, however, that our reliance on GO annotations derived from non-annelid models may  
814 obscure uncharacterised earthworm heat-stress genes. Native to South-East Asia, where  
815 soils often exceed 30 °C, *A. gracilis* nevertheless survives temperatures above the cocoon-  
816 viability threshold of related species (Johnston and Herrick 2019). Instead of heat-stress  
817 pathways, our data highlight transcriptional, epigenetic, and miRNA signatures linked to  
818 hypoxia, pathways governing circulatory and neural development, and epidermal  
819 remodelling, suggesting that O<sub>2</sub> depletion and high CO<sub>2</sub>, rather than heat per se, drive its  
820 adaptive response in volcanic soils.

821

## 822 Conclusion

823 *Amyntas gracilis* earthworms were reciprocally transplanted between non-degassing and  
824 degassing soils, the latter having elevated temperatures, CO<sub>2</sub> emissions, O<sub>2</sub> depletion, and  
825 altered metal concentration profiles including higher Cu, Pb and Zn. RNAseq, miRNaseq,  
826 and MeDIP-Seq profiles were generated to assess functional changes in the response of  
827 these earthworms to extreme conditions. Three main differential tests were used to assess  
828 adaptive and general environmental responses. *A. gracilis* was found to have highly  
829 methylated gene-bodies, with variable gene-component rates, and a clear relationship  
830 between mean expression levels and methylation. Independent functional enrichments of  
831 significant gene-based differences generated by the three data comparisons identified a  
832 consistent set of adaptive pathways that contributed to the plastic traits involved in  
833 adaptation.

834 Earthworm genome methylation was found to be variable, suggesting a degree of  
835 stochasticity with functional plasticity. The identified miRNA networks showed a much higher  
836 relative earthworm site origin effect profile, relative to the transplant destination effect than  
837 did gene expression, suggesting expression sculpting via repression networks may act as a  
838 persistent functional memory within individuals exposed to environmental extremes. Among  
839 functional pathways, epithelial remodelling was identified as a physiological response and  
840 also independently as a functional signature in multiple omics datasets. This finding confirms  
841 this change as an acclimation response of *A. gracilis* to volcanic degassing soils. Circulatory  
842 system morphogenesis and angiogenesis were also repeatedly identified as functional  
843 acclimatisation responses, as was neuron development. Genes linked to these adaptive  
844 pathways were epigenetically modified to a far greater extent in earthworms experiencing  
845 environmental change (i.e. MV and VM treatments), regardless of the type of change. Signal  
846 transduction overall exhibited both a strong methylation response and gene expression

847 profile changes. Metal accumulation was increased in degassing soils, and metal ion  
848 transporters were independently functionally identified as an acclimatisation response to  
849 degassing conditions.

850 Future studies should integrate comparative genomics of metal-detoxification gene families  
851 across earthworm species and experimentally quantify their inducible expression and  
852 methylation dynamics under controlled metal challenges, thereby resolving the relative  
853 contributions of metal tolerance and hypoxia acclimation to extreme-soil colonisation.

854 As critical ecosystem-service providers (Fonte, et al. 2023), annelids play a central role in  
855 soil formation, nutrient cycling, and carbon sequestration. By elucidating the molecular  
856 mechanisms that may underpin adaptive plasticity in *A. gracilis*, a framework is established  
857 for leveraging growing genomic and epigenomic resources to predict which species are likely  
858 to withstand or succumb to environmental extremes. This enhanced understanding will  
859 facilitate the development of molecular biomarkers for resilience or vulnerability, guide  
860 conservation priorities, and inform bioindicator design for monitoring ecosystem health under  
861 accelerating climate change.

862

### 863 Acknowledgements

864 This work was funded by UKRI's Natural Environment Research Council  
865 (Grant NE/I026022/1). O.R. was supported by a UKRI GW4+ DTP studentship  
866 (NE/L002434/1). M.N. received a Marie Curie Fellowship (FP7-IEF-GA-2012-329690). L.C.  
867 was supported by a Horizon2020 Marie Skłodowska-Curie Individual Fellowship  
868 (MSCA-IF-2014-GF-660378) and is currently funded by the Portuguese Foundation for  
869 Science and Technology (FCT; CEECIND/01986/2017). D.S. was funded through an IMP  
870 award from the UK Centre for Ecology & Hydrology Institutional Fund (Project 09221). We  
871 note with deep sadness that Professors Mike Bruford and Andrew John Morgan passed  
872 away during the preparation of this manuscript; their substantial contributions and enduring  
873 legacy remain integral to this work. This study was also supported by the strategic plan of  
874 the Centre for Functional Ecology, Science for People and the Planet (CFE) with the  
875 references UIDB/04004/2025 and UIDP/04004/2025, and by the strategic plan of the  
876 Associate Laboratory TERRA [LA/P/0092/2020] (<https://doi.org/10.54499/LA/P/0092/2020>).

### 877 Data availability

878 All data used in this study have been deposited in the NCBI database under BioProject  
879 accession number PRJNA513445.

880

881    [References](#)

- 882    Alakarppa E, Salo HM, Valledor L, Cañal MJ, Häggman H, Vuosku J. 2018. Natural variation of DNA  
883    methylation and gene expression may determine local adaptations of Scots pine populations. *Journal of Experimental Botany* 69:5293-5305.
- 884    Andersen AC, Flores JF, Hourdez S. 2006. Comparative branchial plume biometry between two  
885    extreme ecotypes of the hydrothermal vent tubeworm *Ridgeia piscesae*. *Canadian Journal of Zoology-Revue Canadienne De Zoologie* 84:1810-1822.
- 886    Anderson C, Cunha L, Sechi P, Kille P, Spurgeon D. 2017. Genetic variation in populations of the  
887    earthworm, *Lumbricus rubellus*, across contaminated mine sites. *BMC Genetics* 18:97.
- 888    Arnold BE, Hodson ME, Charnock J, Peijnenburg W. 2008. Comparison of subcellular partitioning,  
889    distribution, and internal speciation of Cu between Cu-tolerant and naive populations of  
890    *Dendrodrilus rubidus* Savigny. *Environmental Science & Technology* 42:3900-3905.
- 891    Arnold R, Hodson M. 2007. Effect of time and mode of depuration on tissue copper concentrations  
892    of the earthworms *Eisenia andrei*, *Lumbricus rubellus* and *Lumbricus terrestris*. *Environmental Pollution* 148:21-30.
- 893    Bagnato E, Viveiros F, Pacheco J, D'agostino F, Silva C, Zanon V. 2018. Hg and CO<sub>2</sub> emissions from  
894    soil diffuse degassing and fumaroles at Furnas Volcano (São Miguel Island, Azores): Gas flux and  
895    thermal energy output. *Journal of Geochemical Exploration* 190:39-57.
- 896    Banchroft J, Stevens A, Turner D. 1996. Theory and practice of histological techniques. 4th Edn New  
897    York. London, San Francisco, Tokyo: Churchill Livingstone.
- 898    Bartel DP. 2018. Metazoan MicroRNAs. *Cell* 173:20-51.
- 899    Baubron JC, Mathieu R, Miele G. 1991. Measurement of gas flows from soils in volcanic areas: the  
900    accumulation method. . International Conference on Active Volcanoes and Risk Mitig; Napoli.
- 901    Bhambri A, Dhaunta N, Patel SS, Hardikar M, Bhatt A, Srikantham N, Shridhar S, Vellarikkal S, Pandey  
902    R, Jayarajan R, et al. 2018. Large scale changes in the transcriptome of *Eisenia fetida* during  
903    regeneration. *Plos One* 13.
- 904    Bolger AM, Lohse M, Usadel B. 2014. Trimmomatic: a flexible trimmer for Illumina sequence data.  
905    *Bioinformatics* 30:2114-2120.
- 906    Briones M, Álvarez-Otero R. 2018. Body wall thickness as a potential functional trait for assigning  
907    earthworm species to ecological categories. *Pedobiologia* 67:26-34.
- 908    Bushnell B. 2014. BBMap: A Fast, Accurate, Splice-Aware Aligner. 9th Annual Genomics of Energy &  
909    Environment Meeting.; March 17-20; United States.
- 910    Cai Y, Yu X, Hu S, Yu J. 2009. A brief review on the mechanisms of miRNA regulation. *Genomics Proteomics Bioinformatics*  
911    147:147-154.
- 912    Camacho C, Coulouris G, Avagyan V, Ma N, Papadopoulos J, Bealer K, Madden TL. 2009. BLAST plus :  
913    architecture and applications. *Bmc Bioinformatics* 10.
- 914    Chang AJ, Bargmann CI. 2008. Hypoxia and the HIF-1 transcriptional pathway reorganize a neuronal  
915    circuit for oxygen-dependent behavior in *Caenorhabditis elegans*. *Proceedings of the National Academy of Sciences of the United States of America* 105:7321-7326.
- 916    Chiodini G, Cioni R, Guidi M, Raco B, Marini L. 1998. Soil CO<sub>2</sub> flux measurements in volcanic and  
917    geothermal areas. *Applied Geochemistry* 13:543-552.
- 918    Cunha L, Campos I, Montiel R, Rodrigues A, Morgan AJ. 2011. Morphometry of the epidermis of an  
919    invasive megascolecid earthworm (*Amyntas gracilis*, Kinberg 1867) inhabiting actively volcanic  
920    soils in the Azores archipelago. *Ecotoxicology and Environmental Safety* 74:25-32.
- 921    Cunha L, Montiel R, Novo M, Orozco-terWengel P, Rodrigues A, Morgan AJ, Kille P. 2014. Living on a  
922    volcano's edge: genetic isolation of an extremophile terrestrial metazoan. *Heredity* 112:132-142.
- 923    Daniel O, Kohli L, Bieri M. 1996. Weight gain and weight loss of the earthworm *Lumbricus terrestris*  
924    L. at different temperatures and body weights. *Soil Biology and Biochemistry* 28:1235-1240.

- 930 Du Q, Luu P-L, Stirzaker C, Clark SJ. 2015. Methyl-CpG-binding domain proteins: readers of the  
931 epigenome. *Epigenomics* 7:1051-1073.
- 932 Edwards CA, Bohlen PJ. 1996. *The Biology and Ecology of Earthworms*. London, UK: Chapman and  
933 Hall.
- 934 Feinberg AP, Irizarry RA. 2010. Stochastic epigenetic variation as a driving force of development,  
935 evolutionary adaptation, and disease. *Proceedings of the National Academy of Sciences of the  
936 United States of America* 107:1757-1764.
- 937 Ferreira T, Gaspar JL, Viveiros F, Marcos M, Faria C, Sousa F. 2005. Monitoring of fumarole discharge  
938 and CO<sub>2</sub> soil degassing in the Azores: contribution to volcanic surveillance and public health risk  
939 assessment. *Annals of Geophysics* 48:787-796.
- 940 Folmer O, Black M, Hoeh W, Lutz R, Vrijenhoek R. 1994. DNA primers for amplification of  
941 mitochondrial cytochrome c oxidase subunit I from diverse metazoan invertebrates. *Molecular  
942 Marine Biology and Biotechnology* 3:294-299.
- 943 Fonte SJ, Hsieh M, Mueller ND. 2023. Earthworms contribute significantly to global food production.  
944 *Nature Communications* 14:5713.
- 945 Friedländer MR, Mackowiak SD, Li N, Chen W, Rajewsky N. 2012. miRDeep2 accurately identifies  
946 known and hundreds of novel microRNA genes in seven animal clades. *Nucleic Acids Research* 40:37-  
947 52.
- 948 Friedman RC, Farh KK, Burge CB, Bartel DP. 2009. Most mammalian mRNAs are conserved targets  
949 of microRNAs. *Genome Research* 19:92-105.
- 950 Gaspar J, Queiroz G, Ferreira T, Medeiros A, Goulart C, Medeiros J. 2015. Earthquakes and volcanic  
951 eruptions in the Azores region: geodynamic implications from major historical events and  
952 instrumental seismicity. In: Guest JE, Duncan, A.M., Barriga, F.J.A.S., Chester, D.K. , editor. *Volcanic  
953 Geology of São Miguel Island (Azores Archipelago)*. London: Geological Society of London Memoir. p.  
954 33-49.
- 955 Gatzmann F, Falckenhayn C, Gutekunst J, Hanna K, Raddatz G, Carneiro VC, Lyko F. 2018. The  
956 methylome of the marbled crayfish links gene body methylation to stable expression of poorly  
957 accessible genes. *Epigenetics & Chromatin* 11.
- 958 Geeleher P, Huang RS, Gamazon ER, Golden A, Seoighe C. 2012. The regulatory effect of miRNAs is a  
959 heritable genetic trait in humans. *BMC Genomics* 13.
- 960 Griffiths-Jones S, Grocock RJ, van Dongen S, Bateman A, Enright AJ. 2006. miRBase: microRNA  
961 sequences, targets and gene nomenclature. *Nucleic Acids Research* 34:D140-D144.
- 962 Griffiths-Jones S, Saini HK, van Dongen S, Enright AJ. 2008. miRBase: tools for microRNA genomics.  
963 *Nucleic Acids Research* 36:D154-D158.
- 964 Guynes K, Sarre LA, Carrillo-Baltodano AM, Davies BE, Xu L, Liang Y, Martín-Zamora FM, Hurd PJ, de  
965 Mendoza A, Martín-Durán JM. 2024. Annelid methylomes reveal ancestral developmental and aging-  
966 associated epigenetic erosion across Bilateria. *Genome Biology* 25.
- 967 Haas BJ, Papanicolaou A, Yassour M, Grabherr M, Blood PD, Bowden J, Couger MB, Eccles D, Li B,  
968 Lieber M, et al. 2013. De novo transcript sequence reconstruction from RNA-seq using the Trinity  
969 platform for reference generation and analysis. *Nature Protocols* 8:1494-1512.
- 970 Höckner M, Dallinger R, Stürzenbaum SR. 2015. Metallothionein gene activation in the earthworm  
971 (*Lumbricus rubellus*). *Biochemical and Biophysical Research Communications* 460:537-542.
- 972 Holt C, Yandell M. 2011. MAKER2: an annotation pipeline and genome-database management tool  
973 for second-generation genome projects. *Bmc Bioinformatics* 12.
- 974 Huang CD, Shen ZQ, Yue SZ, Jia L, Wang RP, Wang K, Qiao YH. 2023. Genetic evidence behind the Cd  
975 resistance of wild *Metaphire californica*: The global RNA regulation rather than specific mutation of  
976 well-known gene. *Environmental Pollution* 336.
- 977 Huang DW, Sherman BT, Tan Q, Kir J, Liu D, Bryant D, Guo Y, Stephens R, Baseler MW, Lane HC, et al.  
978 2007. DAVID Bioinformatics Resources: expanded annotation database and novel algorithms to  
979 better extract biology from large gene lists. *Nucleic Acid Research* 35:W169-175.

- 980 ISO IOFS. 2005. Soil quality – Determination of pH. In. Geneva: International Organization for  
981 Standardization.
- 982 Jeltsch A, Jurkowska RZ. 2014. New concepts in DNA methylation. Trends in Biochemical Sciences  
983 39:310-318.
- 984 Johnston MR, Herrick BM. 2019. Cocoon heat tolerance of Pheretimoid earthworms *Amyntas*  
985 *tokioensis* and *Amyntas agrestis*. American Midland Naturalist 181:299-309.
- 986 Kajitani R, Toshimoto K, Noguchi H, Toyoda A, Ogura Y, Okuno M, Yabana M, Harada M, Nagayasu E,  
987 Maruyama H, et al. 2014. Efficient de novo assembly of highly heterozygous genomes from whole-  
988 genome shotgun short reads. Genome Research 24:1384-1395.
- 989 Keller TE, Han P, Yi SV. 2016. Evolutionary transition of promoter and gene body DNA methylation  
990 across invertebrate-vertebrate boundary. Molecular Biology and Evolution 33:1019-1028.
- 991 Kille P, Andre J, Anderson C, Ang HN, Bruford MW, Bundy JG, Donnelly R, Hodson ME, Juma G, Lahive  
992 E, et al. 2013. DNA sequence variation and methylation in an arsenic tolerant earthworm population.  
993 Soil Biology & Biochemistry 57:524-532.
- 994 Klok C, Zorn M, Koolhaas JE, Eijsackers HJP, van Gestel CAM. 2006. Does reproductive plasticity in  
995 *Lumbricus rubellus* improve the recovery of populations in frequently inundated river floodplains?  
996 Soil Biology & Biochemistry 38:611-618.
- 997 Klupczynska EA, Ratajczak E. 2021. Can forest trees cope with climate change?-Effects of DNA  
998 methylation on gene expression and adaptation to environmental change. International Journal of  
999 Molecular Sciences 22.
- 1000 Kozomara A, Birgaoanu M, Griffiths-Jones S. 2019. miRBase: from microRNA sequences to function.  
1001 Nucleic Acids Research 47:D155-D162.
- 1002 Kumari T, Phogat D, Jakhar N, Shukla V. 2024. Effectiveness of copper oxychloride coated with iron  
1003 nanoparticles against earthworms. Scientific reports 14:23150.
- 1004 Langdon CJ, Pearce TG, Meharg AA, Semple KT. 2003. Inherited resistance to arsenate toxicity in two  
1005 populations of *Lumbricus rubellus*. Environmental Toxicology and Chemistry 22:2344-2348.
- 1006 Langmead B, Trapnell C, Pop M, Salzberg SL. 2009. Ultrafast and memory-efficient alignment of short  
1007 DNA sequences to the human genome. Genome Biology 10.
- 1008 Lewis BP, Burge CB, Bartel DP. 2005. Conserved seed pairing, often flanked by adenosines, indicates  
1009 that thousands of human genes are microRNA targets. Cell 120:15-20.
- 1010 Li H, Handsaker B, Wysoker A, Fennell T, Ruan J, Homer N, Marth G, Abecasis G, Durbin R, Genome  
1011 Project Data P. 2009. The Sequence Alignment/Map format and SAMtools. Bioinformatics 25:2078-  
1012 2079.
- 1013 Liebers R, Rassoulzadegan M, Lyko F. 2014. Epigenetic regulation by heritable RNA. PLOS Genetics  
1014 10.
- 1015 Lindquist S, Craig EA. 1988. The heat-shock proteins. Annual review of genetics 22:631-677.
- 1016 Lockwood BL, Julick CR, Montooth KL. 2017. Maternal loading of a small heat shock protein increases  
1017 embryo thermal tolerance in *Drosophila melanogaster*. Journal of Experimental Biology 220:4492-  
1018 4501.
- 1019 Lokk K, Modhukur V, Rajashekhar B, Märtens K, Mägi R, Kolde R, Koltsina M, Nilsson TK, Vilo J,  
1020 Salumets A, et al. 2014. DNA methylome profiling of human tissues identifies global and tissue-  
1021 specific methylation patterns. Genome Biology 15.
- 1022 Lopienska-Biernat E, Stryinski R, Dmitryjuk M, Wasilewska B. 2019. Infective larvae of *Anisakis*  
1023 *simplex* (Nematoda) accumulate trehalose and glycogen in response to starvation and temperature  
1024 stress. Biology Open 8.
- 1025 Love MI, Huber W, Anders S. 2014. Moderated estimation of fold change and dispersion for RNA-seq  
1026 data with DESeq2. Genome Biology 15.
- 1027 Luo MM, Sun LM, Hu J. 2009. Neural detection of gases - carbon dioxide, oxygen - in vertebrates and  
1028 invertebrates. Current Opinion in Neurobiology 19:354-361.

- 1029 Maegawa S, Hinkal G, Kim HS, Shen LL, Zhang L, Zhang JX, Zhang NX, Liang SD, Donehower LA, Issa  
1030 JPJ. 2010. Widespread and tissue specific age-related DNA methylation changes in mice. *Genome*  
1031 *Research* 20:332-340.
- 1032 Mandrioli M. 2007. A new synthesis in epigenetics: towards a unified function of DNA methylation  
1033 from invertebrates to vertebrates. *Cellular and Molecular Life Sciences* 64:2522-2524.
- 1034 Mannello F, Medda V, Atonti G. 2011. Hypoxia and neural stem cells: from invertebrates to brain  
1035 cancer stem cells. *International Journal of Developmental Biology* 55:569-581.
- 1036 Martindale JL, Holbrook NJ. 2002. Cellular response to oxidative stress: Signaling for suicide and  
1037 survival. *Journal of Cellular Physiology* 192:1-15.
- 1038 Mendes EG, Nonato EF. 1957. The respiratory metabolism of tropical earthworms II. Studies on the  
1039 cutaneous respiration. *Boletim da Faculdade de Filosofia, Ciências e Letras, Universidade de São*  
1040 *Paulo. Zoologia* 21:153-166.
- 1041 Monahan-Earley R, Dvorak AM, Aird WC. 2013. Evolutionary origins of the blood vascular system and  
1042 endothelium. *Journal of Thrombosis and Haemostasis* 11:46-66.
- 1043 Morgan AJ, Kille P, Stürzenbaum SR. 2007. Microevolution and ecotoxicology of metals in  
1044 invertebrates. *Environmental Science & Technology* 41:1085-1096.
- 1045 Morgan JE, Morgan AJ. 1990. The distribution of cadmium, copper, lead, zinc and calcium in the  
1046 tissues of the earthworm *Lumbricus rubellus* sampled from one uncontaminated and 4 polluted soils.  
1047 *Oecologia* 84:559-566.
- 1048 Newbold LK, Robinson A, Rasnaca I, Lahive E, Soon GH, Lapiet E, Oughton D, Gashchak S, Beresford  
1049 NA, Spurgeon DJ. 2019. Genetic, epigenetic and microbiome characterisation of an earthworm  
1050 species (*Octolasion lacteum*) along a radiation exposure gradient at Chernobyl. *Environmental*  
1051 *Pollution* 255.
- 1052 Novo M, Cunha L, Maceda-Veiga A, Talavera JA, Hodson ME, Spurgeon D, Bruford MW, Morgan AJ,  
1053 Kille P. 2015. Multiple introductions and environmental factors affecting the establishment of  
1054 invasive species on a volcanic island. *Soil Biology & Biochemistry* 85:89-100.
- 1055 Novo M, Lahive E, Diez-Ortiz M, Spurgeon DJ, Kille P. 2020. Toxicogenomics in a soil sentinel  
1056 exposure to Zn nanoparticles and ions reveals the comparative role of toxicokinetic and  
1057 toxicodynamic mechanisms. *Environmental Science-Nano* 7:1464-1480.
- 1058 Perez R, Aron S. 2023. Protective role of trehalose in the Namib desert ant, *Ocymyrmex robustior*.  
1059 *Journal of Experimental Biology* 226.
- 1060 Perry I, Hernadi SB, Cunha L, Short S, Marchbank A, Spurgeon DJ, Orozco-terWengel P, Kille P. 2022.  
1061 Molecular insights into high-altitude adaption and acclimatisation of Aporrectodea caliginosa. *Life*  
1062 *Science Alliance* 5.
- 1063 Reiber CL, McGaw IJ. 2009. A review of the open and closed circulatory systems: New terminology  
1064 for complex invertebrate circulatory systems in light of current findings. *International Journal of*  
1065 *Zoology*. 2009: 301284 |.
- 1066 Rieger RM, Purschke G. 2005. The coelom and the origin of the annelid body plan. *Hydrobiologia*  
1067 535:127-137.
- 1068 Rowell DL. 1994. *Soil Science: Methods and Applications*. Harlow, UK: Longman Scientific and  
1069 Technical.
- 1070 Sarda S, Zeng J, Hunt BG, Yi SV. 2012. The evolution of invertebrate gene body methylation.  
1071 *Molecular Biology and Evolution* 29:1907-1916.
- 1072 Schachtman DP, Goodger JQD. 2008. Chemical root to shoot signaling under drought. *Trends in Plant*  
1073 *Science* 13:281-287.
- 1074 Schoville SD, Barreto FS, Moy GW, Wolff A, Burton RS. 2012. Investigating the molecular basis of  
1075 local adaptation to thermal stress: population differences in gene expression across the  
1076 transcriptome of the copepod *Tigriopus californicus*. *Bmc Evolutionary Biology* 12.
- 1077 Shukla S, Kavak E, Gregory M, Imashimizu M, Shutinoski B, Kashlev M, Oberdoerffer P, Sandberg R,  
1078 Oberdoerffer S. 2011. CTCF-promoted RNA polymerase II pausing links DNA methylation to splicing.  
1079 *Nature* 479:74-79.

- 1080 Silva C, Viveiros F, Ferreira T, Gaspar JL, Allard P. 2015. Diffuse soil emanations of radon and hazard  
1081 implications at Furnas Volcano, São Miguel Island (Azores). In: Gaspar JL, Guest JE, Duncan AM,  
1082 Barriga FJAS, Chester DK, editors. *Volcanic Geology of São Miguel Island (Azores Archipelago)*:  
1083 Geological Society of London. p. 0.
- 1084 Silverman-Gavrila LB, Lu TZ, Prashad RC, Nejatbakhsh N, Charlton MP, Feng ZP. 2009. Neural  
1085 phosphoproteomics of a chronic hypoxia model-*Lymnaea stagnalis*. *Neuroscience* 161:621-634.
- 1086 Simao FA, Waterhouse RM, Ioannidis P, Kriventseva EV, Zdobnov EM. 2015. BUSCO: assessing  
1087 genome assembly and annotation completeness with single-copy orthologs. *Bioinformatics* 31:3210-  
1088 3212.
- 1089 Srut M, Drechsel V, Hockner M. 2017. Low levels of Cd induce persisting epigenetic modifications  
1090 and acclimation mechanisms in the earthworm *Lumbricus terrestris*. *Plos One* 12.
- 1091 Suzuki MM, Kerr ARW, De Sousa D, Bird A. 2007. CpG methylation is targeted to transcription units  
1092 in an invertebrate genome. *Genome Research* 17:625-631.
- 1093 Swart E, Martell E, Svendsen C, Spurgeon DJ. 2022. Soil ecotoxicology needs robust biomarkers: A  
1094 meta-analysis approach to test the robustness of gene expression-based biomarkers for measuring  
1095 chemical exposure effects in soil invertebrates. *Environmental Toxicology and Chemistry* 41:2124-  
1096 2138.
- 1097 Talavera JA, Cunha L, Arévalo JR, Talavera IP, Kille P, Novo M. 2020. Anthropogenic disturbance and  
1098 environmental factors drive the diversity and distribution of earthworms in São Miguel Island  
1099 (Azores, Portugal). *Applied Soil Ecology* 145.
- 1100 Viljoen SA, Reinecke AJ. 1992. The temperature requirements of the epigeic earthworm species  
1101 *Eudrilus eugeniae* (Oligochaeta) - a laboratory study. *Soil Biology and Biochemistry* 24:1345-1350.
- 1102 Viveiros F, Baldoni E, Massaro S, Stocchi M, Costa A, Caliro S, Chiodini G, Andrade C. 2023. Quantification of CO<sub>2</sub> degassing and atmospheric dispersion at Caldeiras da Ribeira Grande (São  
1103 Miguel Island, Azores). *Journal of Volcanology and Geothermal Research* 438:107807.
- 1104 Viveiros F, Cardellini C, Ferreira T, Caliro S, Chiodini G, Silva C. 2010. Soil CO<sub>2</sub> emissions at Furnas  
1105 volcano, São Miguel Island, Azores archipelago: Volcano monitoring perspectives, geomorphologic  
1106 studies, and land use planning application. *Journal of Geophysical Research: Solid Earth* 115.
- 1107 Viveiros F, Ferreira T, Vieira JC, Silva C, Gaspar JL. 2008. Environmental influences on soil CO<sub>2</sub>  
1108 degassing at Furnas and Fogo volcanoes (São Miguel Island, Azores archipelago). *Journal of  
1109 Volcanology and Geothermal Research* 177:883-893.
- 1110 Viveiros F, Gaspar JL, Ferreira T, Silva C, Marcos M, Hipólito A. 2015. Mapping of soil CO<sub>2</sub> diffuse  
1111 degassing at São Miguel Island and its public health implications. In: Gaspar JL, Guest JE, Duncan  
1112 AM, Barriga FJAS, Chester DK, editors. *Volcanic Geology of São Miguel Island (Azores Archipelago)*:  
1113 Geological Society of London. p. 0.
- 1114 Wang C, Sun Z, Zheng D, Liu X. 2011. Function of mucilaginous secretions in the antibacterial  
1115 immunity system of *Eisenia fetida*. *Pedobiologia* 54:S57-S62.
- 1116 Wang K, Qiao YH, Li HF, Huang CD. 2020. Use of integrated biomarker response for studying the  
1117 resistance strategy of the earthworm *Metaphire californica* in Cd-contaminated field soils in Hunan  
1118 Province, South China. *Environmental Pollution* 260.
- 1119 Wang X, Li A, Wang W, Que H, Zhang G, Li L. 2021. DNA methylation mediates differentiation in  
1120 thermal responses of Pacific oyster (*Crassostrea gigas*) derived from different tidal levels. *Heredity*  
1121 126:10-22.
- 1122 Wilson GA, Beck S. 2016. Computational Analysis and Integration of MeDIP-seq Methylome Data. In:  
1123 Next Generation Sequencing: Advances, Applications and Challenges.: InTechOpen. p. 153-169.
- 1124 Zhao X, Yu H, Kong L, Liu S, Li Q. 2016. High throughput sequencing of small RNAs transcriptomes in  
1125 two *Crassostrea* oysters identifies microRNAs involved in osmotic stress response. *Scientific reports*  
1126 6:22687.
- 1127
- 1128
- 1129

1130

1131 **Figure captions**

1132 Fig. 1. Hill-shaded digital elevation model of São Miguel (Azores) showing the two study  
1133 areas: Furnas caldera with active soil degassing and elevated temperature (V, orange) and  
1134 the non-degassing pasture at Macela on Fogo volcano (M, blue). Coloured arrows trace the  
1135 four transplantation routes used in the 31-day in-situ reciprocal experiment (V → V, V → M,  
1136 M → V, M → M; three replicate mesh-bag mesocosms per route; 10 adult worms per bag).  
1137 Black polygons outline volcanic calderas; stars mark the exact sampling/installation sites;  
1138 scale bar = 5 km. (b) Matrix defining the five statistical contrasts interrogated throughout the  
1139 study. Each contrast pools replicate libraries from the appropriate source (A) and destination  
1140 (B) treatments: (1) Static vs Change (resident vs moved worms), (2) Origin vs Origin  
1141 (degassing vs non-degassing provenance), (3) Destination vs Destination (volcanic vs non-  
1142 volcanic exposure), (4) VM vs VV, and (5) MV vs MM. Colour coding follows panel a; c)  
1143 Omics data sets generated: RNA-Seq (4 treatments × 3 replicates), miRNA-Seq (4 × 3), and  
1144 MeDIP-Seq (4 × 1 pooled replicate). **d)** Numbers of features that changed significantly (Wald  
1145 test, DESeq2; p < 0.05, 0.01 or 0.001) in each contrast for mRNA genes (brown), miRNAs  
1146 (green) and gene-body methylated loci (blue). **e)** Top-ten Gene Ontology (GO-BP level 4)  
1147 clusters from DAVID for the three broad contrasts: (1) *Static vs Change*, (2) *Origin vs Origin*,  
1148 (3) *Destination vs Destination*. Bars show fold-enrichment contributed by RNA-Seq (dark  
1149 green), miRNA target interactions (light green) and MeDIP read counts (blue). Prominent  
1150 clusters include epithelium development, circulatory-system morphogenesis, ion transport,  
1151 neural development and signal transduction, highlighting convergent pathways underlying  
1152 rapid epidermal remodelling and physiological acclimation to volcanic stress.

1153

1154 Fig. 2. Model gene body methylation spatial representation, (a) Interval-based relative read  
1155 depth-of-coverage over a model gene, divided into groups corresponding to geometric mean  
1156 gene expression rank deciles (b) Read-mapping likelihood over a model gene, same data as  
1157 (a) represented as binary probability of (any) methylation (c) Visualisation of the full miRNA  
1158 regulatory network between genes (Pink) and miRNAs (blue); (d) Bar graph of the per-node  
1159 edge count to miRNA to gene interaction relationships.

1160

1161 Fig. 3. “Origin vs Origin” functional enrichment cluster intersection between data sources  
1162 (left) and network-view expansion of merged clusters for a single intersection (right). This  
1163 image shows the miRNA regulatory network for the genes annotation with the term  
1164 ‘GO:0072359–circulatory system development’, the network is spatially organised around  
1165 the GO cellular component terms annotating the cluster, and nodes are coloured by fold-  
1166 change in the relevant test.

1167

1168 Fig. 4. “Destination vs Destination” functional enrichment cluster intersection between data  
1169 sources (left) and network-view expansion of merged clusters for a single intersection (right).  
1170 This image shows the miRNA regulatory network for the genes annotated with the term  
1171 ‘GO:0060429–epithelium development’, the network is spatially organised around the GO  
1172 cellular component terms annotating the cluster, and node are coloured by fold-change in  
1173 the relevant test.

1174

1175 Fig. 5. “Static vs Change” functional enrichment cluster intersection between data sources  
1176 (left) and network-view expansion of merged clusters for a single intersection (right). This  
1177 image shows the miRNA regulatory network for the genes annotated with the term  
1178 ‘GO:0060429–epithelium development’, the network is spatially organised around the GO  
1179 cellular component terms annotating the cluster, and nodes are coloured by fold-change in  
1180 the relevant test.

1181

1182 Fig. 6. Expression changes for the “Destination vs Destination” (left-hand column charts),  
1183 “Origin vs Origin” (Middle column charts) and “Static vs change” (right-hand column charts).  
1184 Data represent the MeDIP, RNAseq and miRNA datasets and select for the largest  
1185 functional annotation cluster intersections from Figures 3-5. For each comparison (major  
1186 column), the left-hand sub-column displays the number of genes showing statistically  
1187 significant changes within each functional annotation cluster. In contrast, the right-hand sub-  
1188 column illustrates the net up- or down-regulation for each cluster by data source.  
1189 Additionally, the bar charts on the far right highlight the top nine terms in each cluster,  
1190 ranked by their enrichment p-values.

1191

1192

1193

1194 Supplementary figure captions

1195

1196 Supplementary Fig. S1. Differential expression test results, effect-size shrunk  $\log_2$  FC  
1197 against normalised sample means for the RNAseq results.

1198

1199 Supplementary Fig. S2. Differential expression test results, effect-size shrunk  $\log_2$  FC  
1200 against normalised sample means for the miRNAseq normalised read count.

1201

1202 Supplementary Fig. S3. Differential expression test results, effect-size shrunk  $\log_2$  FC  
1203 against normalised sample means for the MeDIP-Seq results.

1204

1205 Supplementary Fig. S4. Rapid and bidirectional epidermal remodelling and mass change in  
1206 *Amyntas gracilis* after reciprocal exposure to volcanic and reference soils. **a)** Individual  
1207 body mass before and after 31 days of mesocosm exposure across four treatment groups:  
1208 degassing-native maintained in degassing soil (V→V), degassing-native transplanted to  
1209 reference soil (V→M), reference-native transplanted to degassing soil (M→V), and  
1210 reference-native maintained in reference soil (M→M). Transplants from degassing to  
1211 reference soil (V→M) gained weight, while those moved to degassing soils (M→V) showed  
1212 marked weight loss, reflecting physiological stress. **b)** Representative epidermal histology in  
1213 degassing-native worms (V) before and after exposure to reference soil (V→M). Epidermis  
1214 thickened markedly after relocation to less stressful conditions. **c)** Quantification of epidermis  
1215 thickness across treatment groups at the end of the 31-day experiment. Earthworms  
1216 exposed to degassing soil (V→V, M→V) had significantly thinner epidermis compared to  
1217 those in reference soil (V→M, M→M), regardless of origin. **d)** Representative histology of  
1218 reference-native worms (M) before and after 31 days of exposure to volcanic soils (M→V),  
1219 showing epidermal thinning after exposure to extreme conditions. Black scale bars in panels  
1220 **b** and **d** = 25  $\mu\text{m}$ . Data support epidermal thickness as a plastic and rapidly adjusting  
1221 morphological trait reflecting environmental stress, with coordinated changes in body mass.

1222

1223 Supplementary Fig. S5. Origin vs Origin differential miRNA expression network and  
1224 functional enrichment clusters shows miRNAs (large dots) and genes (small dots) and  
1225 whether or not they are upregulated (blue) or down-regulated (pink). All miRNA shown had a  
1226  $p < 0.05$  significance to its differential expression after fold-change effect size shrinking in  
1227 deseq2.

1228

1229   Supplementary Fig. S6. Destination vs Destination differential miRNA expression network  
1230   and functional enrichment clusters. Shows miRNAs (large dots) and genes (small dots) and  
1231   whether they are upregulated (blue) or down-regulated (pink). All miRNA shown had a  
1232    $p < 0.05$  significance to its differential expression after fold-change effect size shrinking in  
1233   deseq2.

1234   Tables

1235

1236 Table 1. Mean concentrations (mg/kg; mean  $\pm$  SD) of metals measured in soil samples from experimental mesocosms. Conditions represent  
 1237 the four transplant treatments: V-V (degassing-origin earthworms maintained in degassing soil), M-V (non-degassing-origin earthworms  
 1238 exposed to degassing soil), V-M (degassing-origin earthworms exposed to non-degassing soil), and M-M (non-degassing-origin earthworms  
 1239 maintained in non-degassing soil). LoD = Limit of Detection.

Condition	Al	Cr	Cu	Fe	Mn	Ni	Pb	Sr	Ti	Zn
LoD	1.63	2.81	0.36	1.45	0.14	4.16	9.04	0.1	0.63	2.1
V-V	18600 $\pm$ 873.7	17 $\pm$ 3.6	96 $\pm$ 12.1	19516.7 $\pm$ 1662.7	587.2 $\pm$ 55.4	6.2 $\pm$ 1.3	108.2 $\pm$ 14.4	34.7 $\pm$ 4	1074.3 $\pm$ 93.5	351.8 $\pm$ 37.2
M-V	18633.3 $\pm$ 740.9	18.1 $\pm$ 3	100.8 $\pm$ 19.9	14033.3 $\pm$ 6337.9	582.8 $\pm$ 40.4	9.1 $\pm$ 5.6	108.6 $\pm$ 13.5	37.3 $\pm$ 2.8	985.8 $\pm$ 123.6	385.5 $\pm$ 90.4
V-M	22500 $\pm$ 2259.1	8.4	20 $\pm$ 5.1	23816.7 $\pm$ 4138.2	692.8 $\pm$ 65.6	13.2	17.5 $\pm$ 4.2	30.2	3270 $\pm$ 770.8	155.3 $\pm$ 59.6
M-M	23100 $\pm$ 896.3	5.4	20.2 $\pm$ 6.2	24366.7 $\pm$ 3870.7	712.2 $\pm$ 51.8	12.7	17.6 $\pm$ 2	25.2	3266.7 $\pm$ 681.4	173 $\pm$ 79.7

1240

1241

1242 Table 2. Earthworm body matter metal content (mg/kg) is fractionated between metal-rich granules (MGR), soluble material (SOL), and soft  
 1243 matter (INT: tissue fragments, membranes, etc). Different letters show significant differences after a comparison using Tukey HSD ( $p < 0.05$ ).

	Condition	Na	Mg	Al	K	Ca	Ti	Cr	Mn	Fe	Ni	Cu	Zn	Ga	As	Sr	Cd	Pb	Bi
<b>SOL</b>	V_in_V	3123a	1271	27	4229a	4152	25	0.75	35	244ab	1.41	43.43a	190	0.04	1.30b	26.24	7.87a	1.50a	0.07a
	M_in_V	2577ab	1333	29	3479ab	4103	29	0.66	34	316a	1.58	47.35a	209	0.05	2.05ab	44.25	9.82a	1.56a	0.01ab
	V_in_M	2589ab	1737	26	3495ab	3674	33	0.57	44	263ab	0.87	17.49b	211	0.05	1.62ab	37.56	3.16b	0.41b	0.01b
	M_in_M	2309b	1507	26	3117b	3485	27	0.68	43	226b	0.98	15.95b	198	0.05	3.31a	43.88	3.97b	0.19b	0.00b
<b>MRG</b>	V_in_V	1011b	239a	413	1209a	605a	8a	0.21a	13a	73a	0.19	5.49a	47ab	0.12	4.42	7.59	0.46a	1.75a	0.01a
	M_in_V	1195b	192ab	344	1232a	473ab	6ab	0.20a	10ab	73a	0.23	5.26a	52a	0.11	4.08	26.16	0.55a	1.56a	0.00a
	V_in_M	1449a	222a	369	1192a	455b	6ab	0.12b	9b	50ab	0.17	1.60b	35b	0.09	3.92	8.04	0.14b	0.20b	0.00ab
	M_in_M	1415a	170b	296	927b	370b	4b	0.10b	10ab	40b	0.13	1.59b	40ab	0.08	3.62	13.22	0.20b	0.15b	0.00b
<b>INT</b>	V_in_V	15430	1062b	2519a	550ab	7524b	184	10.47	316	2903	8.61b	44.99a	140	1.86a	1.30ab	167.14	0.91ab	32.28a	0.08a
	M_in_V	13930	1719b	2010ab	614a	9659ab	107	9.09	387	3239	6.61b	53.15a	190	1.56ab	1.56a	1096.68	1.40a	34.67a	0.09a
	V_in_M	18561	2741a	1762ab	611a	10258ab	193	14.41	409	2696	48.40a	18.59b	152	1.21ab	0.70c	299.27	0.24b	2.62b	0.01b
	M_in_M	18909	2784a	1124b	411b	10934a	128	8.73	514	2310	37.88ab	14.67b	194	1.01b	0.84bc	857.22	0.34b	2.24b	0.01b
<b>Total</b>	V_in_V	19171	2664b	3025a	5913a	12334	221	11.95	383	3274	10.67ab	96.37a	381	2.07a	7.15	175.43	9.36a	36.52a	0.16a
	M_in_V	17703	3244b	2384ab	5325a	14235	142	9.95	430	3628	8.42b	105.75a	451	1.72ab	7.69	1167.1	11.77a	37.79a	0.10b
	V_in_M	22598	4699a	2157ab	5298a	14387	232	15.1	462	3010	49.44a	37.67b	399	1.36ab	6.24	344.87	3.54b	3.23b	0.02c
	M_in_M	22633	4461a	1446b	4455b	14789	158	9.51	566	2575	38.99ab	32.21b	432	1.14b	7.77	914.32	4.50b	2.57b	0.02c

Supplementary Table S1. Sample sequencing libraries with trimming and alignment rates for the RNAseq, miRNA-seq and MeDIP-Seq libraries.

RNA-Seq Libraries							
Sample	Raw (Read Count)	Trimmed	%	Aligned	%	Gb Raw	Gb Trimmed
V→V.1	22305582	20666302	92.7	17913624	86.7	3.35	3.1
V→V.2	31911228	30025366	94.1	25528676	85	4.79	4.5
V→V.3	32531640	30731750	94.5	26429150	86	4.88	4.61
V→M.1	29123856	27394556	94.1	23594138	86.1	4.37	4.11
V→M.2	34197226	32364024	94.6	27869880	86.1	5.13	4.85
V→M.3	30819382	29063042	94.3	24813578	85.4	4.62	4.36
M→V.1	29724434	27861854	93.7	24121614	86.6	4.46	4.18
M→V.2	33385916	31472080	94.3	27183240	86.4	5.01	4.72
M→V.3	42270714	40075616	94.8	34414400	85.9	6.34	6.01
M→M.1	38009410	35987182	94.7	31246464	86.8	5.7	5.4
M→M.2	36211208	34253562	94.6	29578904	86.4	5.43	5.14
M→M.3	40477494	38548640	95.2	32915512	85.4	6.07	5.78
miRNA-Seq Libraries							
Sample	Raw (Read Count)	Trimmed	%	Aligned	%	Gb Raw	Gb Trimmed
V→V.1	25747134	24292420	94.3	7652639	31.5	3.86	3.64
V→V.2	16981154	16412964	96.7	7157806	43.61	2.55	2.46
V→V.3	26188542	24343821	93	8604909	35.35	3.93	3.65
V→M.1	15078814	14407309	95.5	6559646	45.53	2.26	2.16
V→M.2	21472620	20177299	94	9703776	48.09	3.22	3.03
V→M.3	20634684	19536629	94.7	5664319	29	3.1	2.93
M→V.1	20646086	19669009	95.3	9288720	47.23	3.1	2.95
M→V.2	22016268	20886785	94.9	10574566	50.63	3.3	3.13
M→V.3	22384786	21148899	94.5	7729828	36.55	3.36	3.17
M→M.1	20872376	19547815	93.7	8186318	41.88	3.13	2.93
M→M.2	24970848	23189178	92.9	8180014	35.28	3.75	3.48
M→M.3	28557792	27316670	95.7	7995913	29.27	4.28	4.1
MeDIP-Seq Libraries							
Sample	Raw (Read Count)	Trimmed	%	Aligned	%	Gb Raw	Gb Trimmed
V→V	9150071	8721337	95.3	7888845	90.5	1.37	1.31
V→M	12703975	11969754	94.2	10855396	90.7	1.91	1.8
M→V	14715950	13250605	93.5	12225125	92.3	2.13	1.99
M→M	15477553	14754260	95.3	13469337	91.3	2.32	2.21

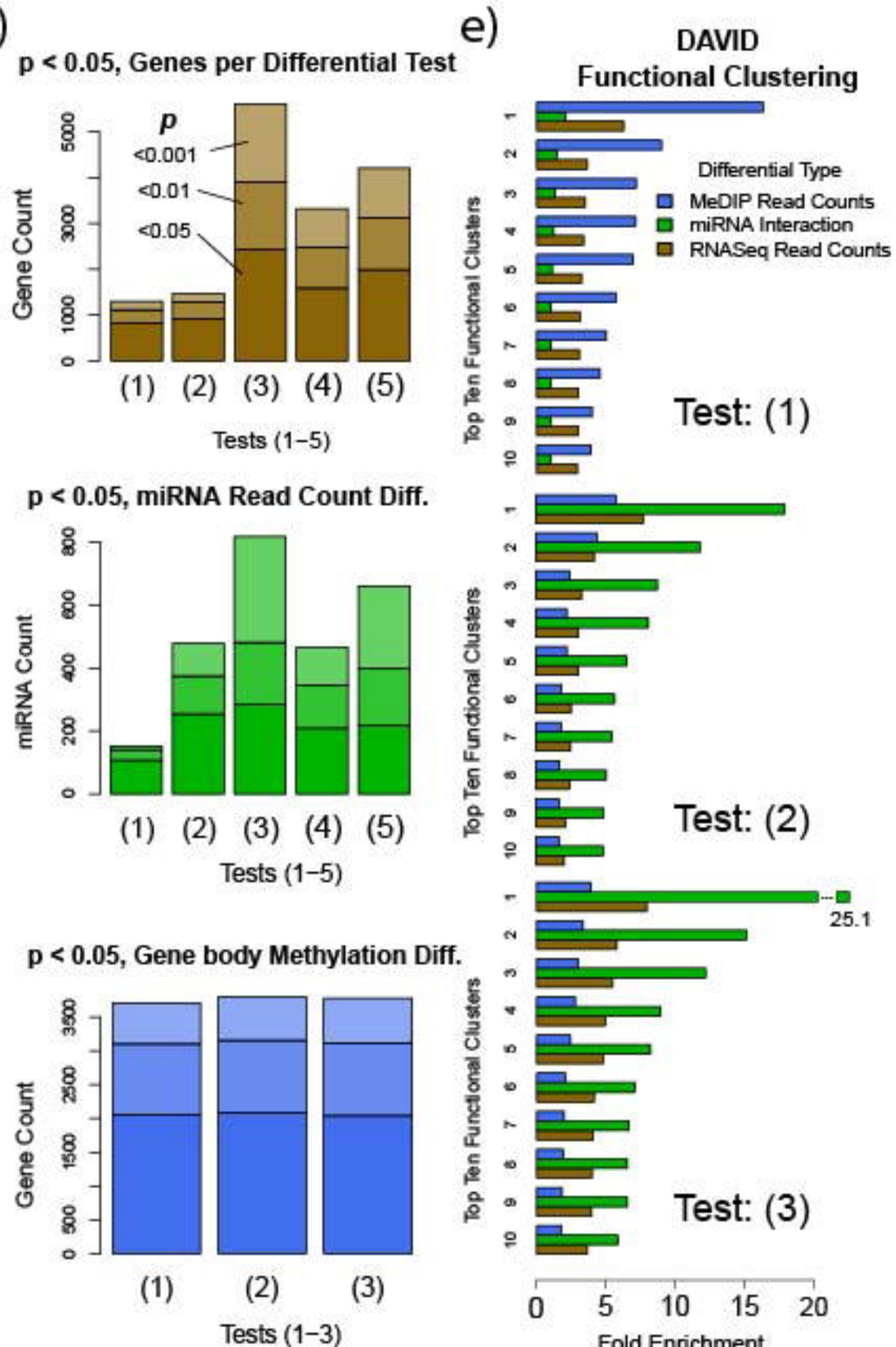
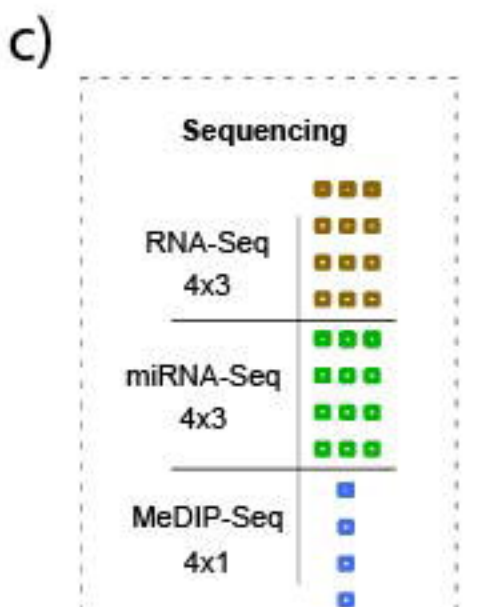
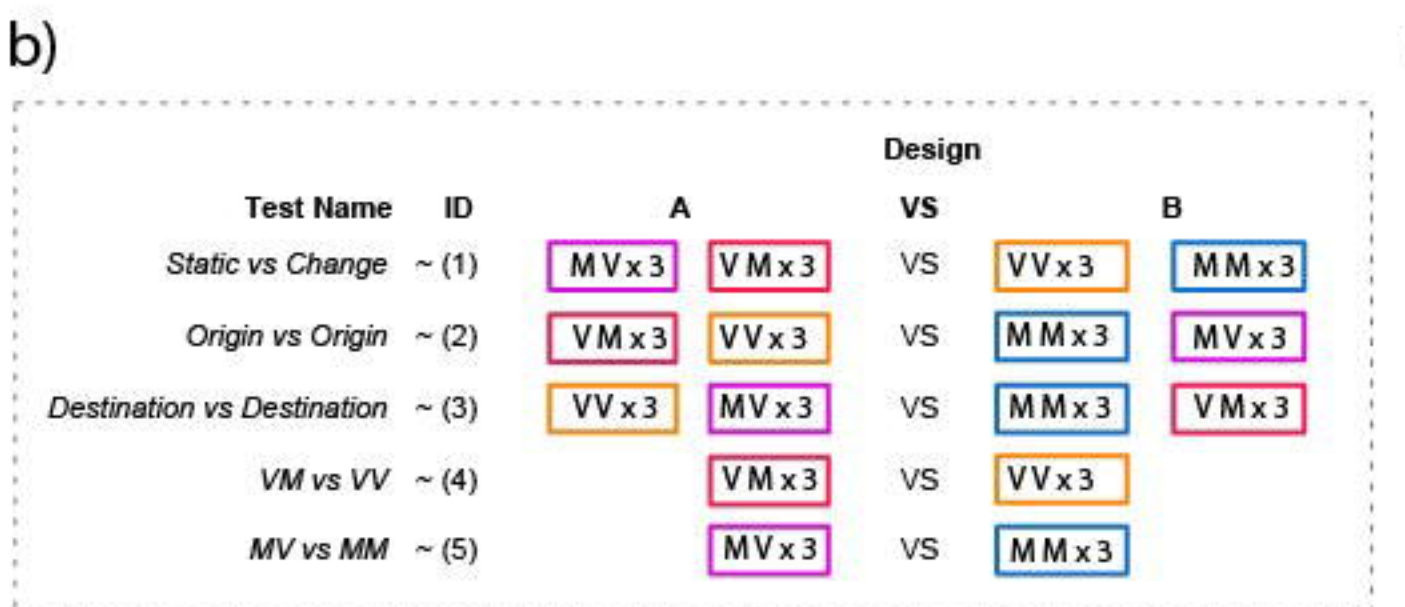
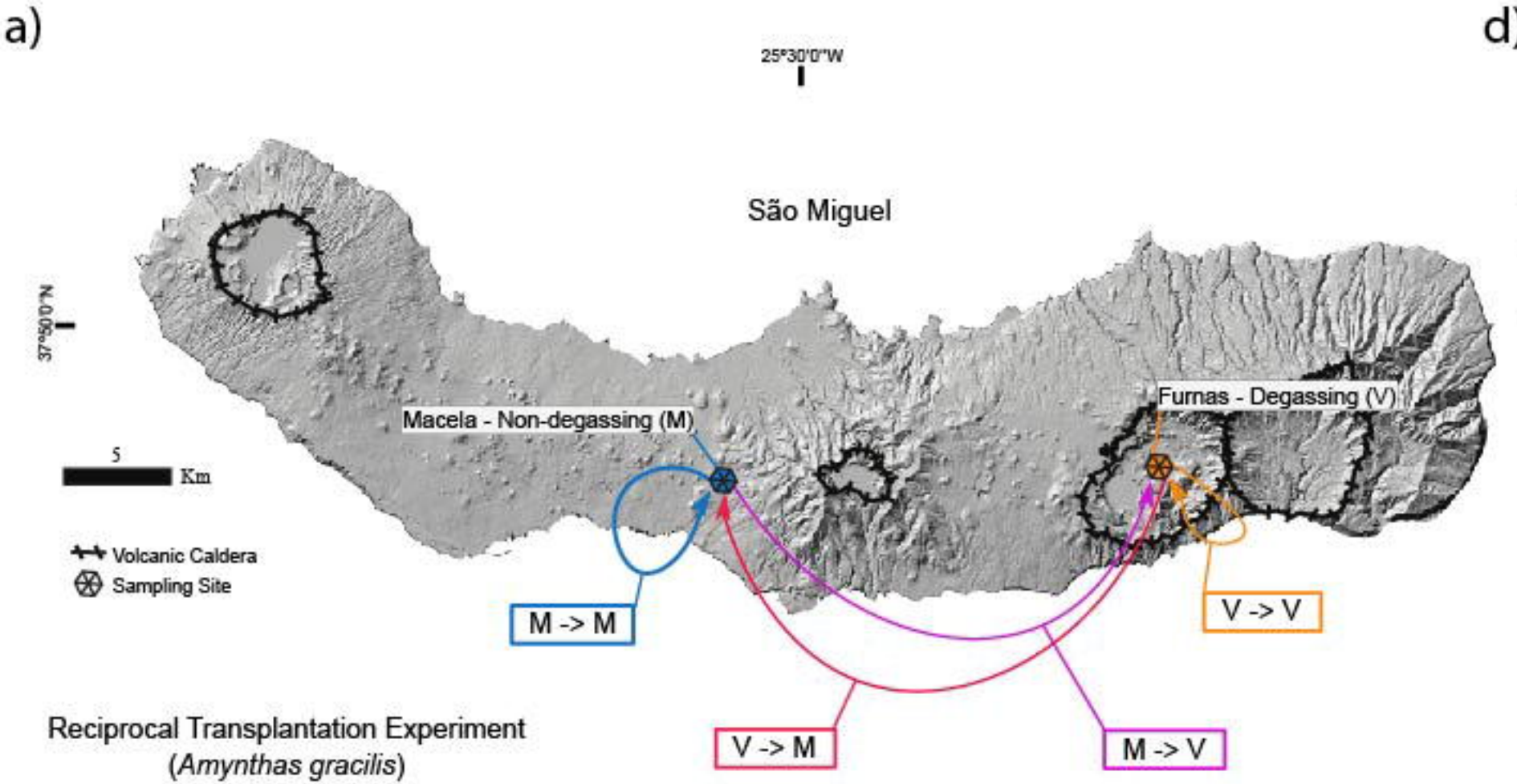
Supplementary Table S2. Gas and temperature conditions at the earthworm sampling and transplant deployment sites.

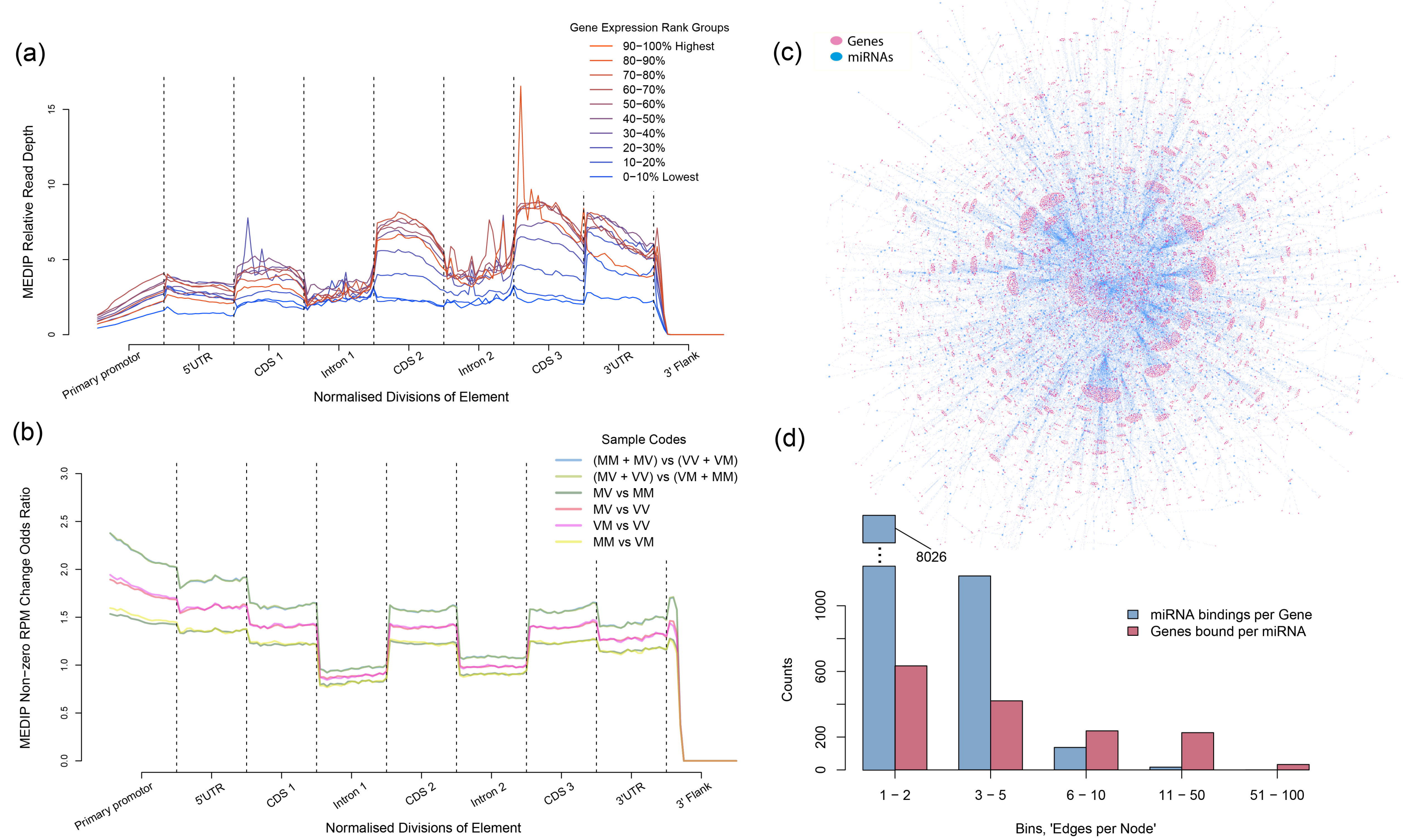
Soil variable	Macela (Non-degassing site)						Furnas (Degassing site)					
	Transplant Site			Collection Site			Transplant Site			Collection Site		
	Mean	Max	Min	Mean	Max	Min	Mean	Max	Min	Mean	Max	Min
CO <sub>2</sub> (vol%) 25 cm	nd	nd	nd	nd	nd	nd	21.5	71.7	4.3	6.7	9.6	1.8
CO <sub>2</sub> (vol%) 50 cm	0.8	2.8	0.1	0.7	2.3	0.2	48.6	96.5	14	6.9	8.8	2.4
CO <sub>2</sub> flow (g m <sup>-2</sup> d <sup>-1</sup> )	19.5	27.5	12.3	15.4	32.4	6.2	181	533	58	19.8	25	12.5
O <sub>2</sub> (vol%) 25 cm	18.1	18.2	17.9	-	-	-	15.7	19.1	6.3	10.7	18.8	3.4
O <sub>2</sub> (vol%) 50 cm	18.5	19.9	13.1	18.8	20	15.6	10.4	17.1	1.4	9.9	18.3	1.2
Temperature °C 25 cm	17.5	17.6	16.2	17	18.9	15.9	35	45.7	28	18.4	19.6	17.9
Temperature °C 50 cm	17	17.6	16.2	17.1	18.8	15.9	37.3	47.3	29.8	17.8	19.3	17.8

Supplementary Table S3. Soil properties in soil samples collected from mesocosms. \* Sample loss.

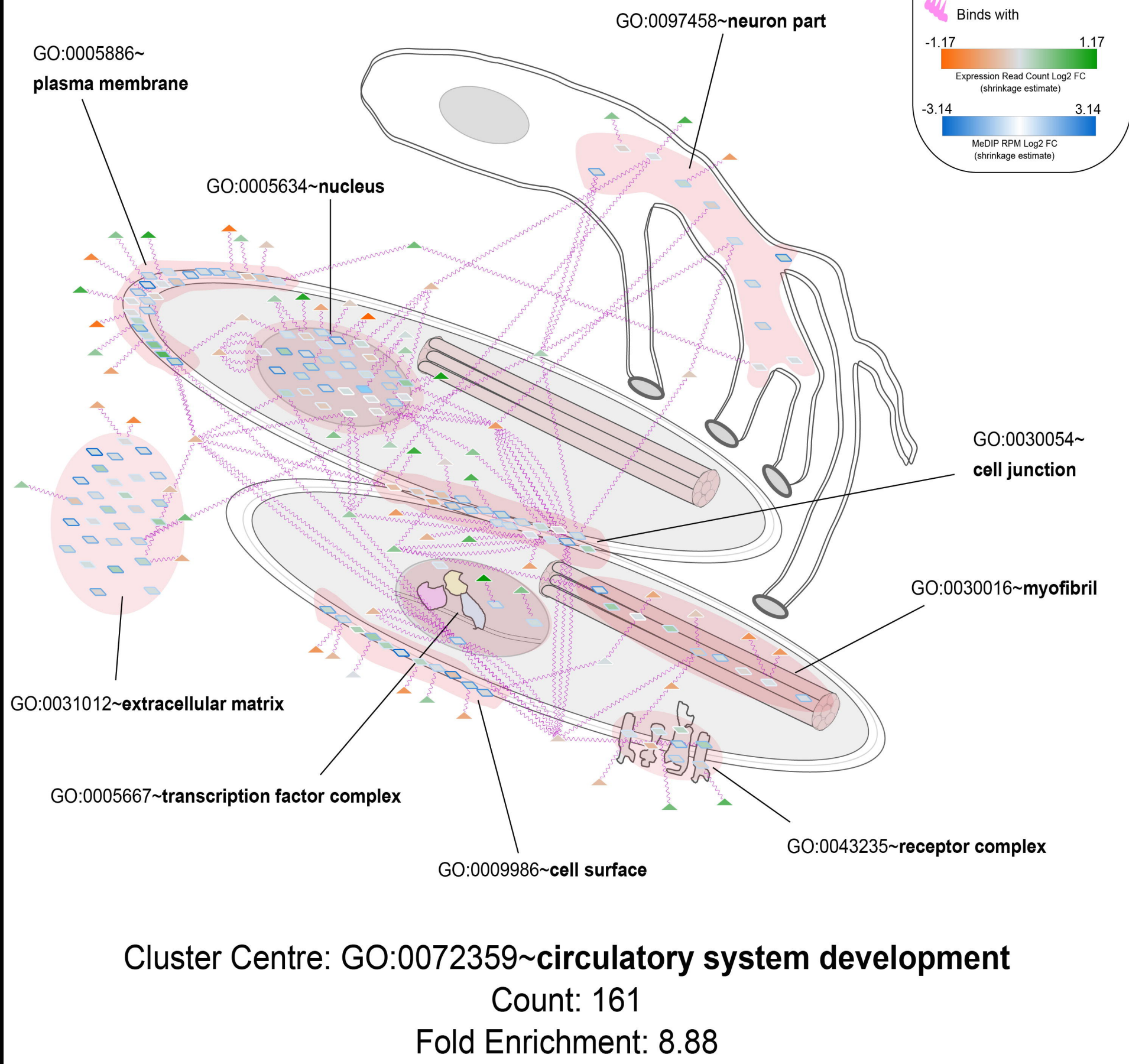
Sample	Clay (%)	Silt (%)	Sand (%)	pH	Soil moisture content (%)	Loss on ignition (%)	Water holding capacity (%)
V→V.1	3	65	35	5.46	4.13	10.74	74.19
V→V.2	2	66	35	5.69	7.47	10.71	78.93
V→V.3	3	71	30	5.24	9.08	12.58	82.93
V→V.4	5	70	29	5.4	5.2	12.64	93.5
V→V.5	2	38	62	5.49	5.04	11.45	79.01
V→V.6	3	66	35	5.83	4.83	10.25	75.43
V→V Avg.	3	62.67	37.67	5.52	5.96	11.4	80.67
M→V.1	3	74	26	5.66	6.1	11.42	74.61
M→V.2	4	76	25	5.43	5.51	11.11	86.15
M→V.3	2	36	64	5.23	10.29	12.12	83.38
M→V.4	3	68	33	5.84	8.08	10.87	85.42
M→V.5	2	55	47	5.46	4.8	10.22	75.81
M→V.6	2	62	40	5.53	5.32	9.89	76.81
M→V Avg.	2.67	61.83	39.17	5.53	6.68	10.94	80.36
V→M.1	1	53	49	5.72	17.44	32.72	140.79
V→M.2	1	54	47	5.6	8.17	24.52	106.36
V→M.3	1	39	62	5.89	6	25	112.2
V→M.4	2	50	51	5.45	13.39	29.37	120.16
V→M.5	2	57	44	5.05	31.68	34.91	119.9
V→M.6	1	62	40	5.65	16.48	23.06	106.4
V→M Avg.	1.33	52.5	48.83	5.56	15.53	28.26	117.63
M→M.1	1	55	47	4.99	22.04	30.4	157.3
M→M.2	1	50	51	5.23	12.92	25.61	103.99
M→M.3	2	54	47	5.81	12.34	25.34	108.61
M→M.4	1	53	49	5.33	22.56	36.7	155.31
M→M.5	1	59	42	6	18.38	21.71	110.57
M→M.6	*	*	*	6.37	5.8	14.42	100.16
M→M Avg.	1.2	54.2	47.2	5.62	15.67	25.7	122.66



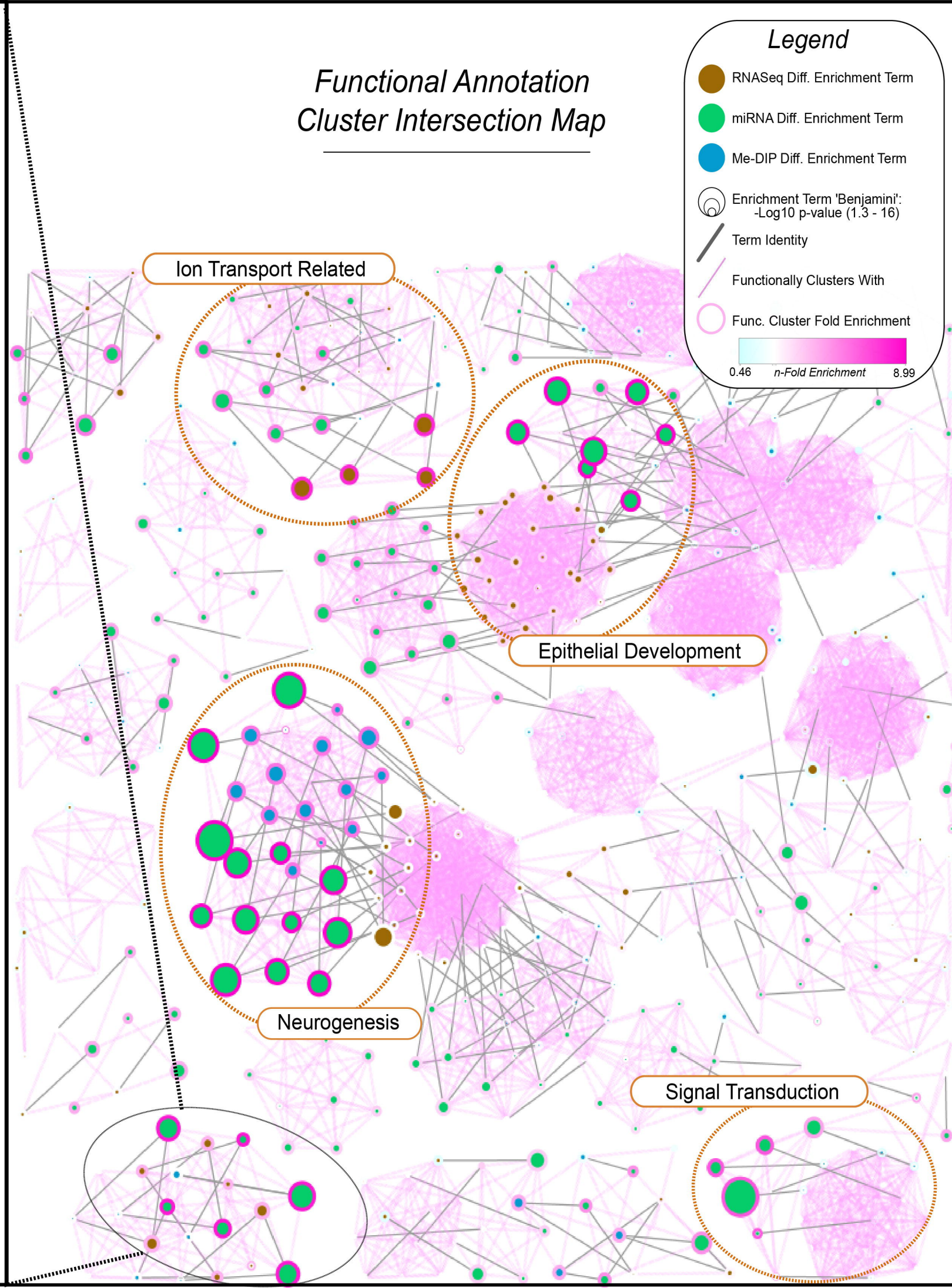




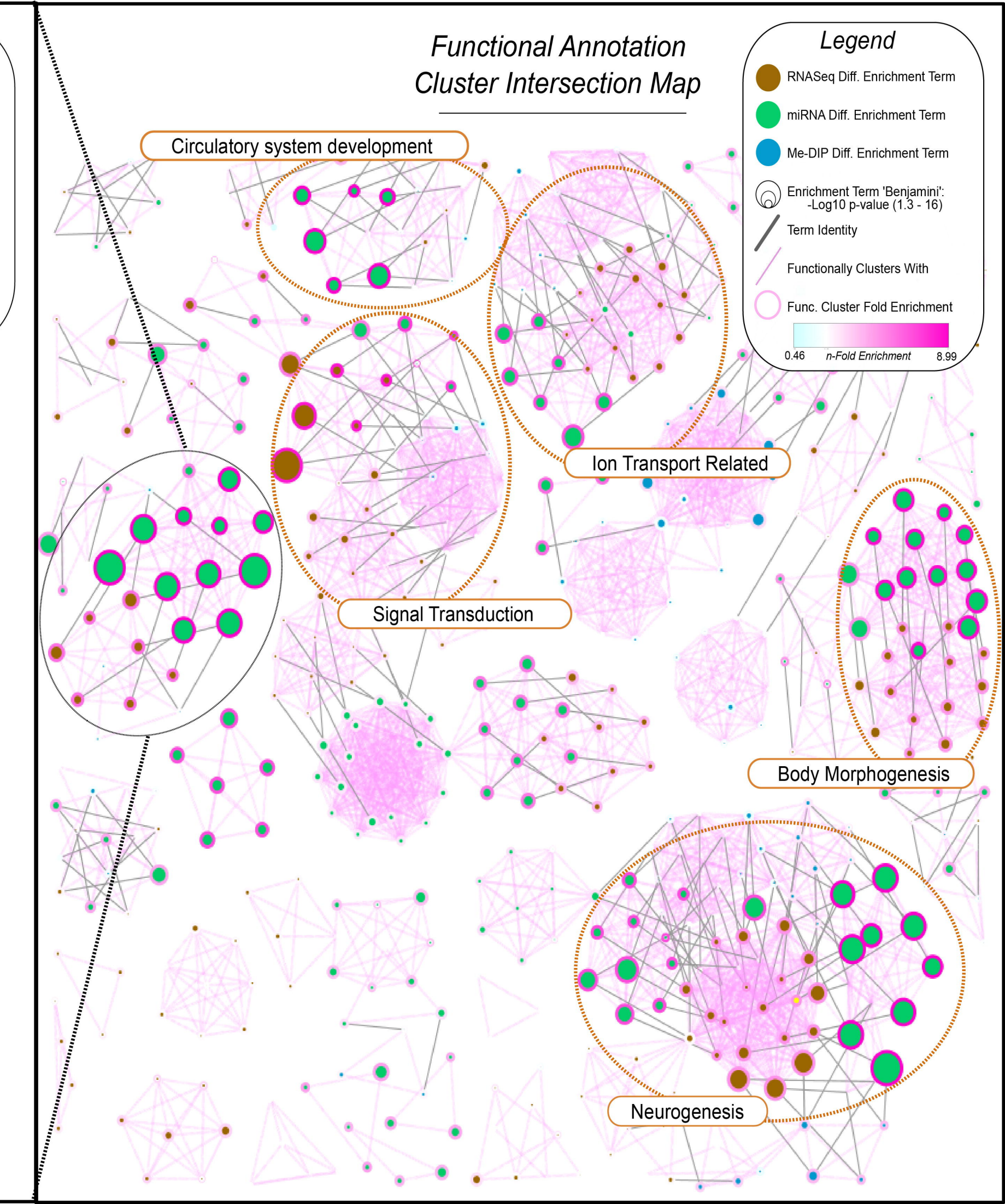
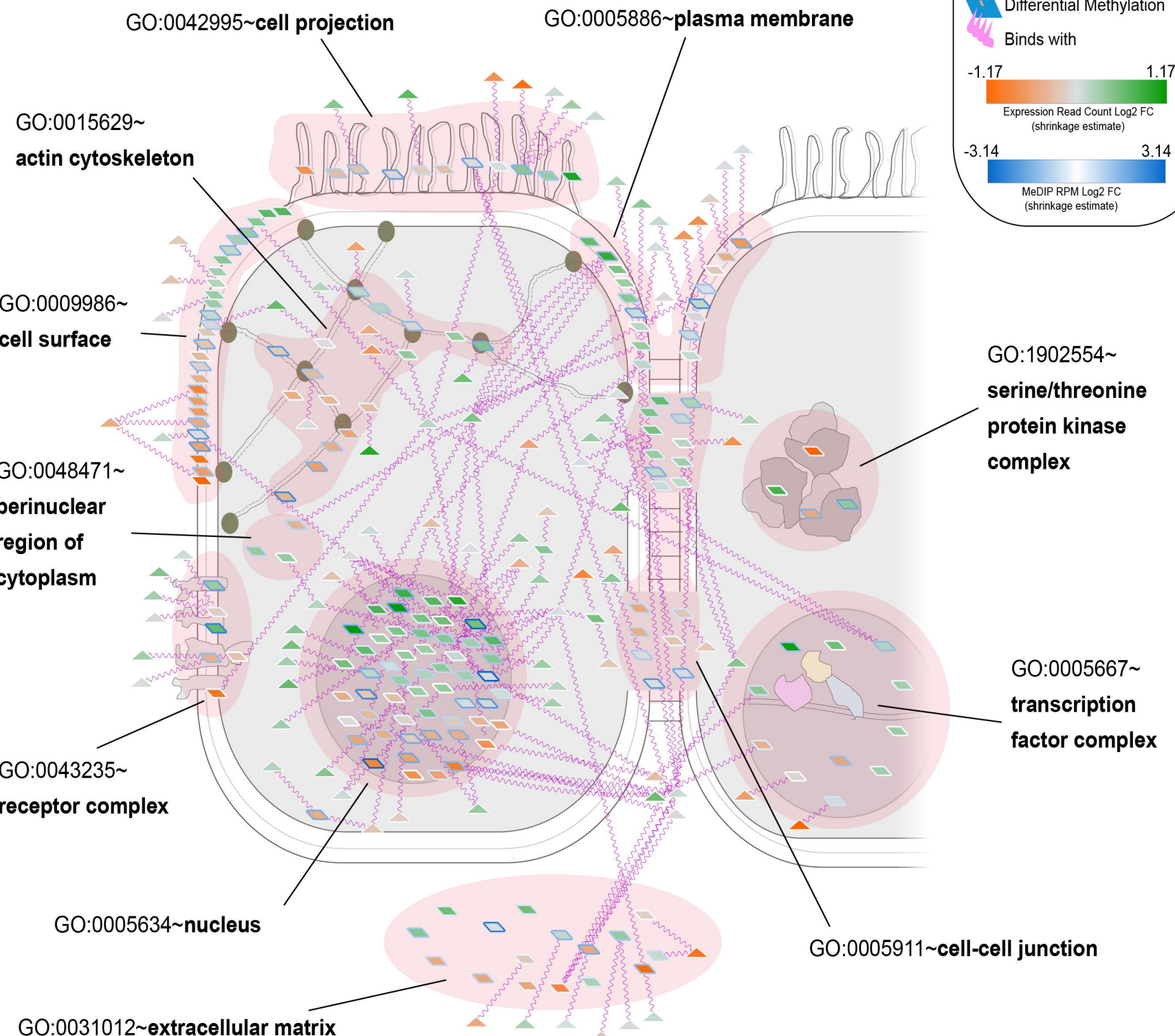
# Origin vs Origin (Furnas vs Macela)



## Functional Annotation Cluster Intersection Map

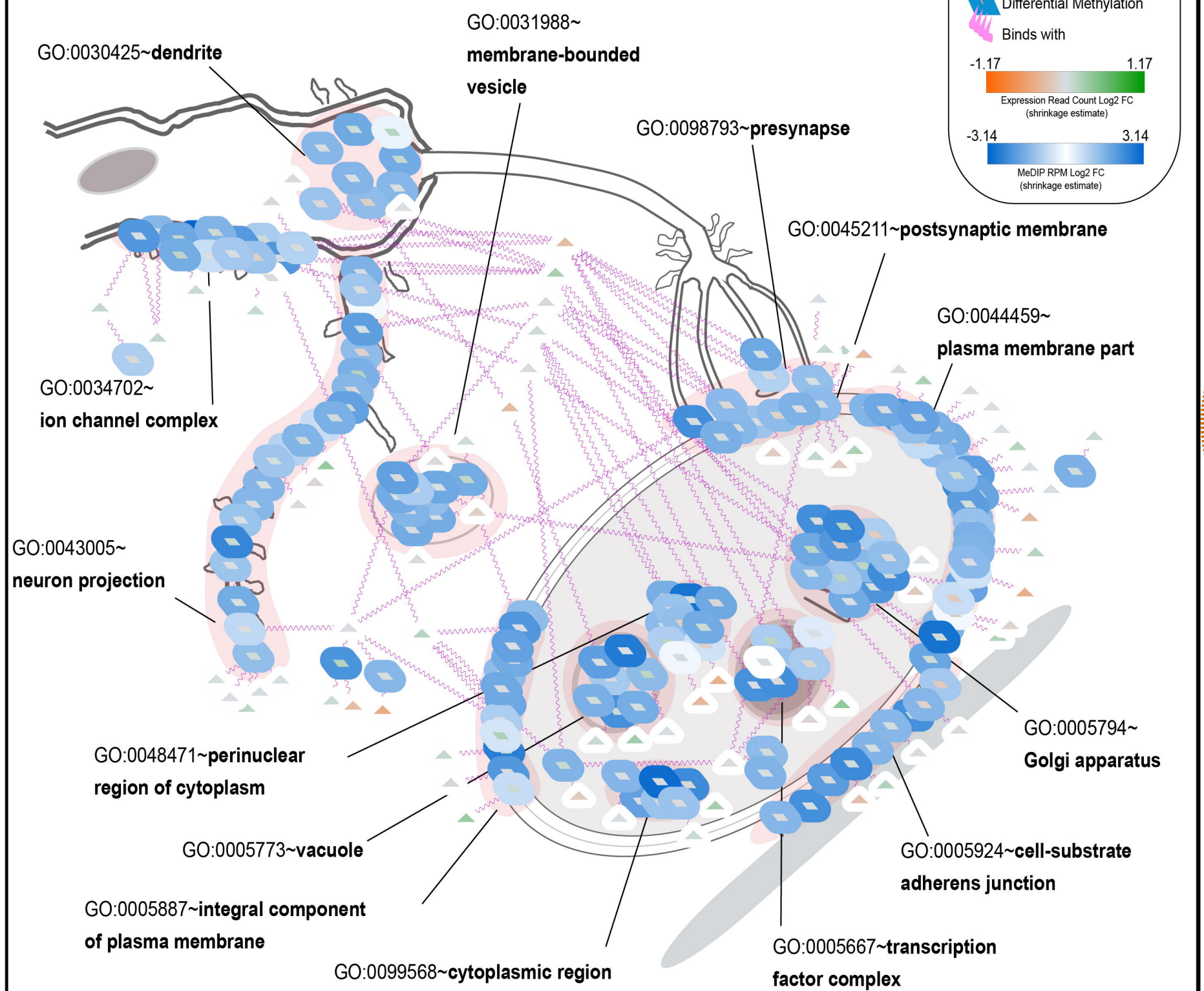


# Destination vs Destination (Furnas vs Macela)



# Stationary vs Change (Same soil vs different soil)

bioRxiv preprint doi: <https://doi.org/10.1101/2025.07.24.666578>; this version posted July 29, 2025. The copyright holder for this preprint (which was not certified by peer review) is the author/funder, who has granted bioRxiv a license to display the preprint in perpetuity. It is made available under aCC-BY 4.0 International license.



## Functional Annotation Cluster Intersection Map

